Summer 2021

Analysis of Gravity for the Crustal Structure of Nepal Himalaya

Kapil Prasad Phuyal
Missouri State University, Kapil456@live.missouristate.edu

ANALYSIS OF GRAVITY FOR THE CRUSTAL STRUCTURE OF NEPAL HIMALAYA

A Master's Thesis

Presented to

The Graduate College of

Missouri State University

In Partial Fulfillment

Of the Requirements for the Degree

Master of Science, Geography and Geology

By

Kapil Prasad Phuyal

July 2021

ANALYSIS OF GRAVITY FOR THE CRUSTAL STRUCTURE OF NEPAL HIMALAYA

Geology, Geography, and Planning

Missouri State University, July 2021

Master of Science

Kapil Prasad Phuyal

ABSTRACT

Nepal Himalaya is situated in the central portion of the seismically active Himalayan Orogenic Belt, which is geologically segmented by four major mega fault structures: Main Frontal Thrust (MFT), Main Boundary Thrust (MBT), Main Central Thrust (MCT), and the South Tibetan Detachment System (STDS). The MFT, MBT, and MCT are part of the basal decollement Main Himalayan Thrust (MHT) which accommodates the convergence between the Indian and Eurasian Plate. The 2015 Gorkha Earthquake occurred within the MHT system, MHT system itself had been seismically locked since the 1934 Nepal-Bihar Earthquake, complicating the geometry depth of MHT. Available land and airborne gravity data were used to determine the general crustal structure of Nepal. The gravity data was processed into a series of gravity anomaly maps such as complete Bouguer gravity, isostatic residual gravity, wavelength filtered gravity, and derivative gravity anomalies which revealed major tectonic boundaries, and the gravity anomalies showed the density variation of the underlying rocks. The derivative map, upward continued map and Euler's deconvolution map indicated the depth of the MHT system ranges from 3 km and 15 km before the locking zone. The less dense area is surrounded by large dense anomaly bodies in the 2015 Gorkha Earthquake region, which can be interpreted as the causes of stress within the region. The north to the south steeper gradient indicates a steeper and deeper Moho towards the north. The geometry and exact location of the MHT profile can be revealed from a 2-D forward gravity model.

KEYWORDS: Main Himalayan Thrust, Nepal Himalaya, 2015 Gorkha Earthquake, Bouguer gravity anomaly, crustal structure

ANALYSIS OF GRAVITY FOR THE CRUSTAL STRUCTURE OF NEPAL HIMALAYA

By

Kapil Prasad Phuyal

A Master's Thesis
Submitted to the Graduate College
Of Missouri State University
In Partial Fulfillment of the Requirements
For the Degree of Master of Science, Geography and Geology

July 2021

Approved:

Dr. Kevin L. Mickus, Distinguished Professor, Thesis Committee Chair

Dr. Melida Gutierrez, Professor, Committee Member

Dr. Douglas R. Gouzie, Professor, Committee Member

Dr. Julie Masterson, Dean of the Graduate College

ACKNOWLEDGEMENTS

I would like to remember every helping hand who help me throughout my graduate studies at Missouri State University. Firstly, I would like to express my deepest gratitude to my advisor, Dr. Kevin L. Mickus, for his valuable guidance during my graduate study from the beginning to this date, which was a vital part of completing my graduate degree. Through his guidance, I can improvise my knowledge of geology and geophysics, and different geophysical tools. I am very thankful with my committee members, Dr. Douglas R. Gouzie and Dr. Melida Gutierrez for their valuable suggestions after reviewing my thesis draft. Their creative comments helped me to improve the quality of my writing and presentation. Similarly, I would like to thank Dr. Gary Michelfelder, and Dr. Xiaomin Qiu for their continued advice to develop a research proposal and research background. Moreover, I am very thankful to my friends from the department, especially Andrea M. Vanne, and Shoukat Ahmed for their help in running different analytical tools.

I would like to express my big thank you to the US- National Geospatial-Intelligence Agency for providing airborne gravity data of my study area. I would also like to thank Santoshi Aryal, my wife, who continuously encourage me to focus on my research and study. Even if, we are in a long-distance relationship for 2 years, she always makes me feel that we are together for each other in every good and bad time. Likewise, I want to express my sincere gratitude to my parents for their unconditional love and supports to achieve every goal in my life.

Finally, thanks also go to the GGP departments for the resources and the information they provide to complete my thesis.

TABLE OF CONTENTS

LIST OF TABLES

LIST OF FIGURES

CHAPTER-1 INTRODUCTION

The Himalayas is a typical example of continent-continent collision in which the Indian plate and Eurasian plate started to collide during the Eocene period and continues until now (Le Fort, 1975; Gansser, 1983; Ni. J., 1989). Despite the different models of Himalayan origin, the underthrusting model is evidenced from many geological and geophysical investigations in which the Indian lithospheric plate underthrust beneath the Eurasian plate at the Himalaya and Southern Tibet (Ni. J., 1989). The northward drift of the Indian plate toward the Eurasian plate is around 5-6 cm per year (Searly, 2013). This drift and the underthrusting are the major causes of the crustal shortening, uplift, and seismicity of the Himalayas (Bilham et al., 1997).

The 2,400 km long Himalayan orogenic belt can be divided into four major structural units as Tethyan Himalayan Sedimentary units, Higher Himalayan Sequence metamorphic rocks, the lesser Himalayan fold-and-thrust belt, and the sub-Himalayan molasses basin (Searle & Treloar, 2019). These structural units are mostly evidenced by the presence of five major fault systems as the South Tibetan Detachment (STD), Main Central Thrust (MCT), Main Boundary Thrust (MBT), Main Frontal Thrust (MFT), and the Main Himalayan Thrust (MHT) (Martin, 2017).

Nepal Himalaya lies in the central segment of the Himalayan Orogenic Belt (Figure 1) covering 800 km out of 2,400 km entire length of Himalaya (Dhakal et al., 2019). This region is further divided into four major structural units from south to north as Sub-Himalaya, Lesser Himalaya, Higher Himalaya, and Tethyan Himalaya (Gansser 1964; Le Fort, 1986; Dhakal et al., 2019). These structures are segmented by the MFT, MBT, MCT, and STD system (Ni and Barazangi, 1984; Zhao and Nelson, 1993). All these faults converge at one detachment structure

along the subduction zone MHT (Ni and Barazangi, 1984; Zhao and Nelson, 1993; Nábělek et al., 2009; Dhakal et al., 2019).

Large magnitude Himalayan earthquakes occur at the plate interface between Indian and Eurasian plates: The Main Himalayan Thrust (MHT plate interface) (Bilham et al., 2001; Zilio et al., 2020). Therefore, the study of the geometry of MHT is crucially important for the crustal structure determination of the Nepal Himalaya region.

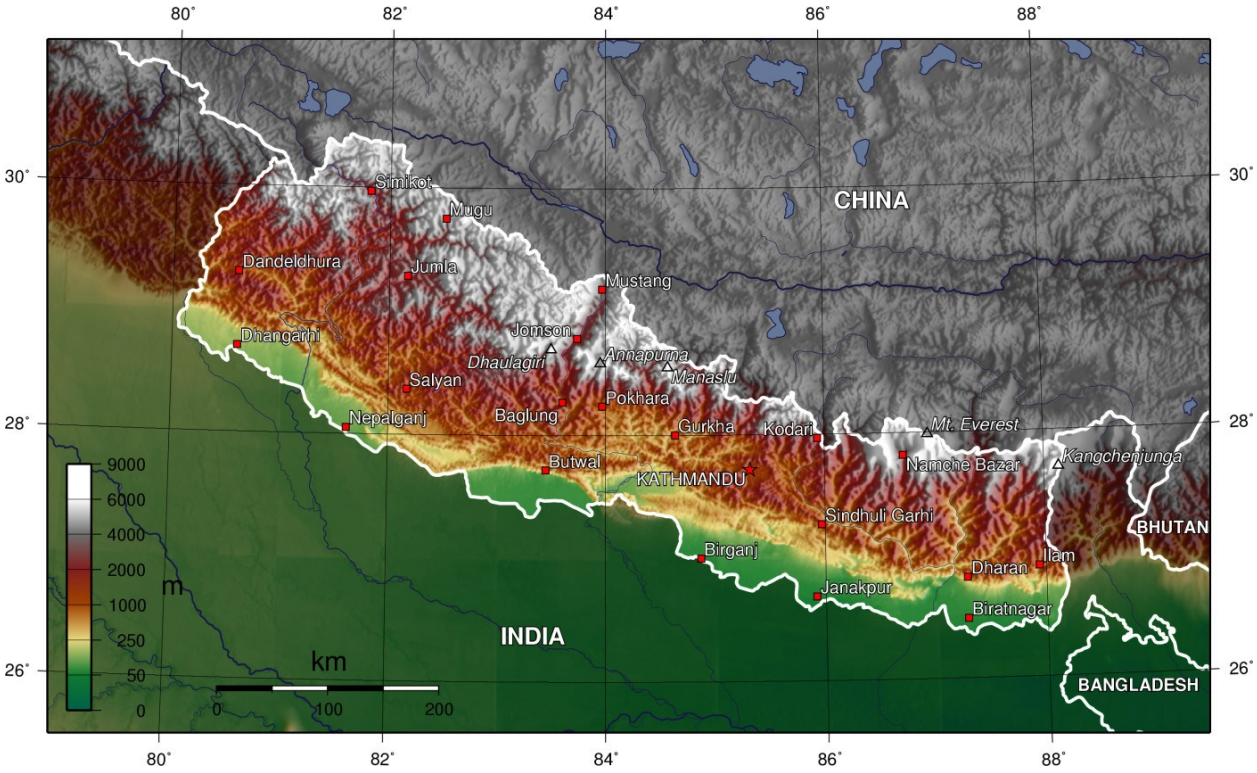

Figure 1 Geographic Elevation Map of Nepal Himalaya. The red-pink shaded region is a range of the Himalayan Orogenic Belt.

Nepal Himalaya lies in the seismically active region of the Himalayan Orogenic Belt (HOB) which has experienced several moderate to large earthquakes in the past (Prakash et al., 2016). The 2015 Gorkha Nepal Earthquake of 7.8 Mw was a recent disastrous event occurred on April 25, 2015 that killed nearly 9,000 people, injured thousands of people, and produced

property damage of an estimated 5 billion dollars (Bilham, 2015). The main earthquake occurred on the southern slope of the Himalaya orogenic belt and formed a 120-140 km long and 80 km wide rupture zone with a dip-slip on the Main Himalayan Thrust (MHT) of 3.5 -5.5 m (Wu et al., 2019). The major epicenter of mainshock and aftershocks are centered in the Central Nepal region (Figure 2).

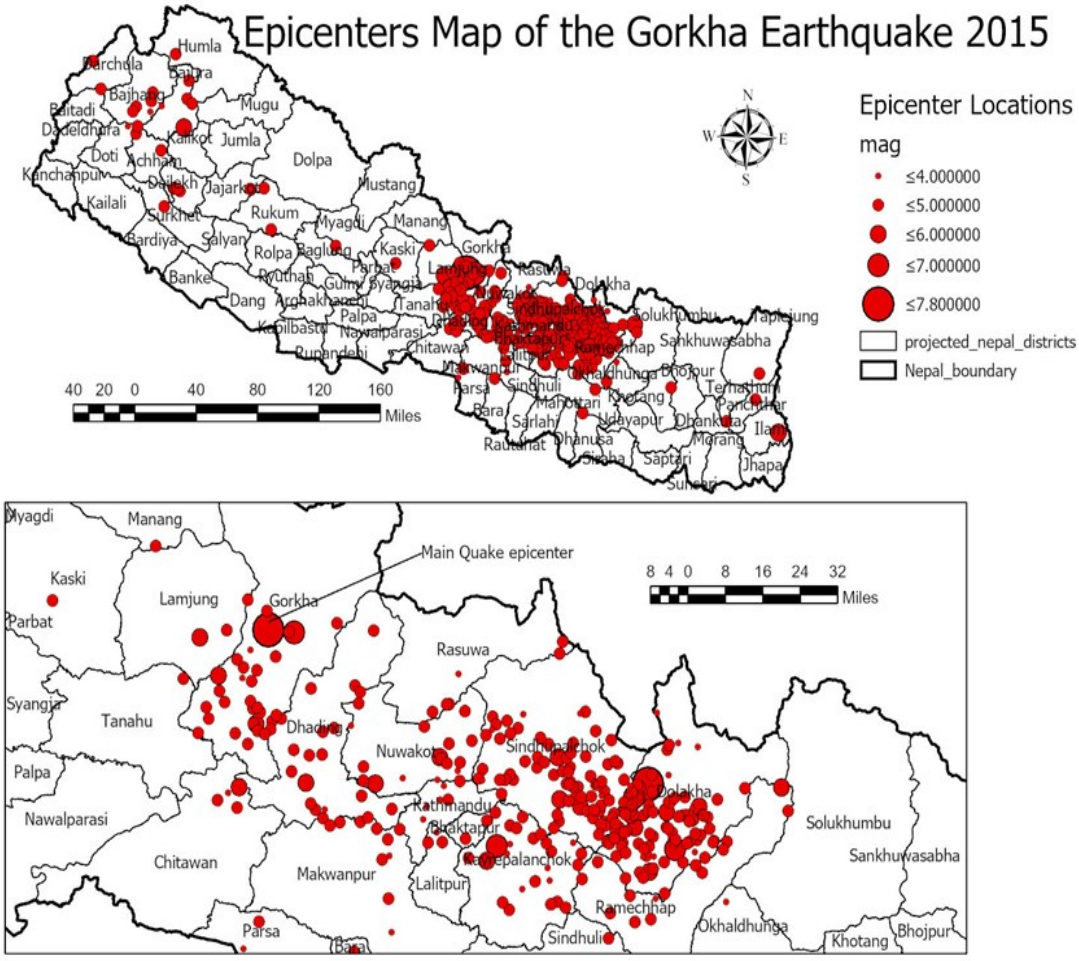

Figure 2 Above: Location of the main event and aftershocks of the 2015 Gorkha Earthquake. Below: Close up of the affected area. The red circle represents the locations of the earthquakes whereas the size of the circle represents the magnitude of the earthquake.

Numerous studies have been conducted on subsurface structure and rupture kinematics of the 2015 Gorkha earthquake region using seismic data (Denolle et al., 2015; Grandin et al., 2015; Wang et al., 2015; Bai et al., 2016; Hubbard et al., 2016; Huang et al., 2017; Bie et al., 2019). Four major findings were gathered from these studies, 1) morphological structure of MHT controlled the rupture length of the 2015 Gorkha earthquake, 2) mainshock occurred on MHT at 18.5 km depth, 3) the rupture velocity was 3.1-3.2 km/s, and 4) the variation in fault orientation of MHT was likely responsible for limiting the size and location of the 2015 Gorkha Earthquake. The study by Chen et al. (2016), Kono (2007), and Cattin et al. (2001). Chen et al. (2016) reviewed the gravity data of the HOB Collision zone between 2010-2013 that showed that the gravity of the 2015 Gorkha Nepal Earthquake source region increased gradually. The gravity change may be related to strain aggregation and possibly mass relocation in a broad source region of the 2015 Gorkha Earthquake. Therefore, gravity data can be used to analyze the crustal structure as well as monitoring the active fault region.

It is reasonable to believe that extended geophysical study beneath the 2015 Gorkha earthquake region using gravity data can help reconstruct the major events that resulted in Himalayan orogeny and ascertain the detailed geometry of the MHT at depth. Cattin et al. (2001) and Kono (2007) researched the crustal structure of central and eastern Nepal using gravity data. These studies gave clues that there is density contrast in MBT and MFT and strain weakening along the MHT. Still, there is a gap in research about the subsurface geometry of the MHT at depth. Two-dimensional (2-D) gravity modeling and profile of topography, free air, and Bourger gravity anomaly changes allow us to determine crustal thickness, degree of isostatic compensation, and amount of crustal thickening (Mickus and Jallouli, 1999). To this purpose, Euler's 3-dimensional (3-D) deconvolution method, as well as 2-D forward gravity model

integration with different map analysis methods including wavelength filter, isostatic residual gravity anomalies, and derivative methods, are used to outline the geometry of the subsurface structure, following the methodology utilized by Duba (2018) and Mickus and Jallouli (1999). At the end of this study a final model accompanying all geologic data, previous seismic constraints, and gravity maps provide information on the crustal structure and tectonic evolution of central Nepal Himalaya.

The principal objective of this study is to investigate and map the lithospheric structure beneath the central Nepal Himalaya region where a devastating earthquake of 7.8 Mw occurred on 25 April 2015. To meet this objective land gravity data, airborne gravity data, and satellite gravity data were collected from various sources. These data were processed and analyzed to draw a series of gravity maps, encompassing Bouguer gravity anomaly, band-pass filtered, horizontal derivatives, and isostatic residual gravity. Euler's 3-D deconvolution method was employed to trace the boundary of the tectonic structure and source body depth.

CHAPTER-2 GEOLOGY AND TECTONICS

2.1 Regional Geology of the Himalaya

Himalaya is an idiosyncratic geological setting in the entire world that consists of rugged topography and a complex geological setup (Sastry and Singh, 2012). It has not any direct continuation either towards the west or the east (Gansser, 1964). The evolution and the rise of the Himalayas have been continuously beholding by the three great antecedent rivers-Indus, Ganga, and Bramhaputra-since 50Ma (Patriat and Achche, 1984; Dhital, 2015). The Himalayan Orogenic Belt (HOB) is the highest orogenic belt on the earth with extensive seismicity which contains the Himalayan mountain range formed by the collision between the Indian and Eurasian Plate. The entire length of the HOB is divided into four tectonostratigraphic units from south to north associated with the bounding faults MFT, MBT, MCT, and STD: Sub-Himalaya, Lesser Himalaya, Higher Himalaya, and Tethyan Himalaya (Yin et al., 2006; Bai et al., 2016). In some literature, the Higher Himalayan sequence rocks are also termed as Greater Himalayan Sequence [Gansser, 1964, 1983; Le Fort, 1975; McQuarrie et al., 2008; Martin, 2017] (Figure 3). A summary and definition of all the major tectonostratigraphy of the Himalayas are shown in Table 1.

The Tethyan Himalayan sequence lies in the southern periphery of the Tibetan plateau which is known as the oldest Himalayan deformation (McQuarrie et al., 2008; Dhital, 2015). This sequence comprises a variety of terrigenous and carbonate sediments like sandstone, siltstones, dolostones, limestones, and shales of age range Cambrian to Eocene (Dhital, 2015). This sequence is mostly located in the northern section of Himalaya and popular for the abundant reserve of organic materials (Dhital, 2015; Singh et al., 2019). The Higher Himalayan sequence

rocks are considered as the hanging wall of the MCT which consists of 5-20 km thick north dipping allochthonous block (Lefort, 1975; Valdiya, 1980). STD system is marked as a boundary between the Tethyan Himalayan sequence and the Higher Himalayan sequence (Godin et al., 2006). The Higher Himalayan Crystallines (HHC) are primarily composed of augen and banded gneiss. It also consists of migmatite, schist, quartzite, and marble altering with Paleozoic granite and tertiary leucogranite. This sequence is also marked as inverted metamorphism at the base and Barrovian type metamorphism at the top where the grade of metamorphism is diminishing continuously towards Sub-Himalaya and sharply attenuate towards the Tethyan sedimentary system (Dhital, 2015).

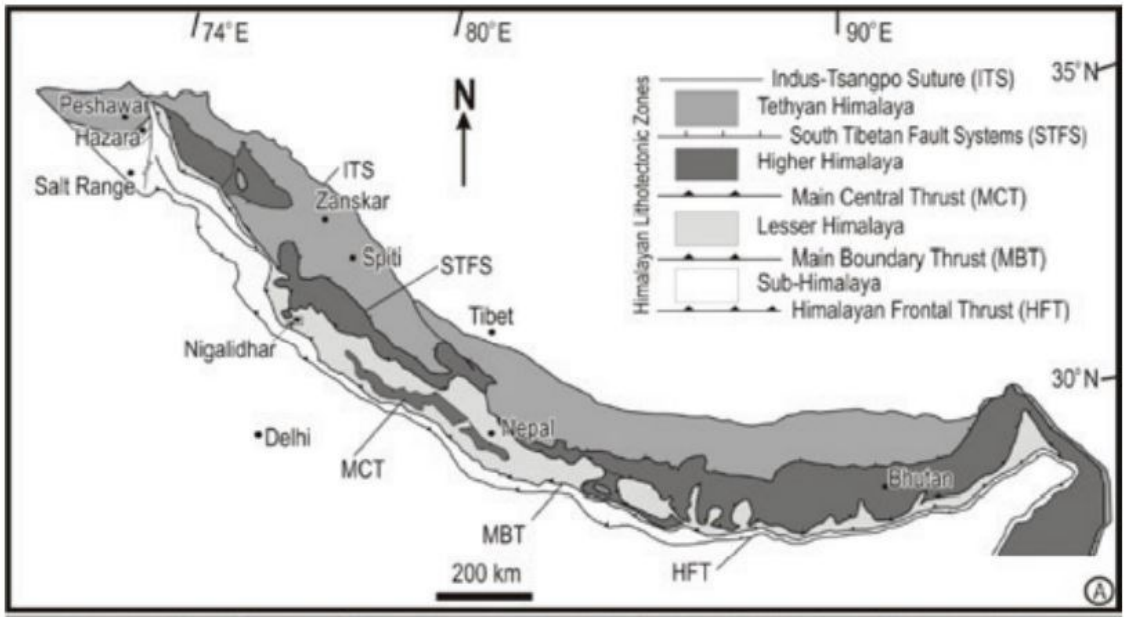

Figure 3 Simplified Geological Map of the Himalaya which comprises the study area (Singh et al., 2019).

The Lesser Himalayan sequences (LHS) are represented by a 60-80 km wide belt which extensively comprises Proterozoic low-grade metamorphic rocks overlined by thrust sheet of

granites and metamorphic rocks (Roy and Purohit, 2018). They are widely exposed in between Sub Himalaya and HHC from south to north. There is a gigantic depositional gap in most of LHS between the Proterozoic rocks and overlying Paleocene-Eocene beds which indicate a long history of non-deposition (Dhital, 2015). This Sequence was considered to have been actively uplifted and thrusted over the Sub Himalaya by MBT, after the termination of the activity along with the MCT during Late Miocene time (Decelles et al., 2000).

The Sub Himalaya stands for the foreland basin developed in front of the rising Himalaya which contains a tertiary rock sequence in between the MBT and HFT (Thakur et al., 2020). The Sub Himalaya Sequences comprise synorogenic sedimentary rocks that were made up of sediments from the Himalayan Mountains during Mid Miocene to Mid Pliocene time (Quade et al., 1995; Decelles et al, 1998; McQuarrie et al., 2008). The Sub Himalayan hills can be easily noticed by observing higher mountains in the north and abrupt elevation change in the south in the Himalayan region (Medicolt and Blanford, 1879).

The major faults of the Himalaya (MCT, MBT, and MFT) all arise from the basal decollement known as the MHT which distinguishes the Himalayan orogenic wedge from the underlying Indian Plate (Zhao et al., 1993; Hauck et al., 1998) (Figure 4). MHT is also considered to connect with a major shallow dipping reflector observed beneath the Tethyan Himalaya (Makovsky et al., 1999; Srivastav and Mitra, 1994).

2.2 Geology of the Nepal Himalayan

Nepal is situated in the central portion of the HOB covering about one-third of the total length of the entire Himalayan arc which consists of contrasting altitude land features (Hagen, 1969; Dhital, 2015). Both the highest mountain of the world, Mount Everest with altitude

8848m, and the deepest defile of the earth, Kaligandaki Gorge reside in Nepal Himalaya. The Nepal Himalaya is extended between the Kumaon Himalaya in the west and the Sikkim-Bhutan Himalaya in the east. The Nepal Himalaya is subdivided into the following five major tectonic zones from south to north (Upreti and Le Fort, 1999; Figure 5). The stratigraphic order is presented below:

Indo-Gangetic Plain (Terai)

----Himalayan Frontal Thrust (HFT) ----

Sub-Himalaya (Siwalik or Churia Group)

---- Main Boundary Thrust (MBT) ----

Lesser Himalaya

---- Main Central Thrust (MCT) ----

Higher Himalaya

---- South Tibetan Detachment System (STDS) ----

Tibetan-Tethys Himalaya

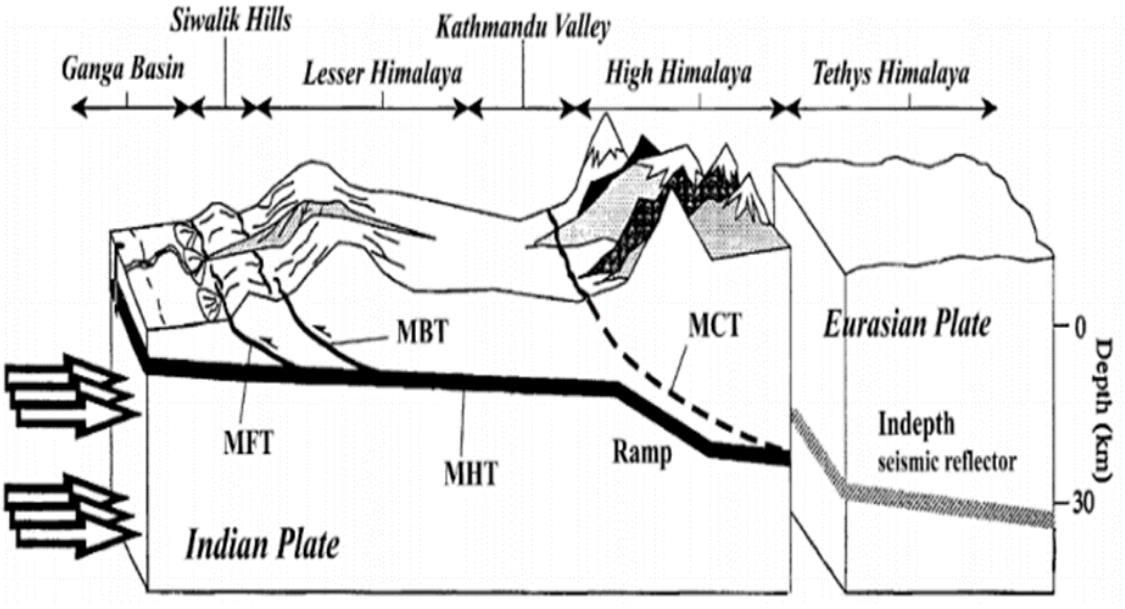

Figure 4 Diagrammatic representation of the major tectonic structures of the Himalayan orogenic belt. MFT-Main Frontal Thrust, MBT-Main Boundary thrust, MCT-Main Central Thrust, MHT-Main Himalayan Thrust (modified after Takada and Matsu'ura, 2007).

Table 1 Summary of major tectonostratigraphic zonation of the Himalaya (Martin, 2017).

Name	Classification Type	Definition
Sub Himalaya (Siwalik group)	Structural position	Sedimentary rocks between Main Frontal Thrust and Main Boundary Thrust.
Lesser Himalaya	Structural position	Rocks located between Main Boundary Thrust and Main Central Thrust.
Higher Himalaya	Structural and metamorphic	Rocks are located in the hanging wall of the MCT and high-grade.
Tethyan Himalaya	Structural and Metamorphic	Rocks located in the hanging wall of the MCT and low-grade.

2.2.1 Indo-Gangetic Plain (Terai): The Terai zone represents the northern edge of the Indo-Gangetic Plain (Figure 5) and forms the southernmost tectonic division, which is limited by MFT at the north comprising Pleistocene to recent alluvium with an average thickness of about 1500m (Upreti,1999). This zone is exposed in three different locations of the southern end of the Nepal Himalaya where boulder to clay sediment deposits can be observed (Hagen, 1969). This region is further subdivided into three zones respectively from south to north as Lower Terai or Gangetic Alluvium, Middle Terai or Marshy zone, and Inner Terai or Bhabar Zone. The

uppermost Bhabhar is composed of boulders and pebbles, the Middle part (Marshy zone) is made up of sands, and the lowermost Gangetic Alluvium consists of dominant clay (Dhital, 2015).

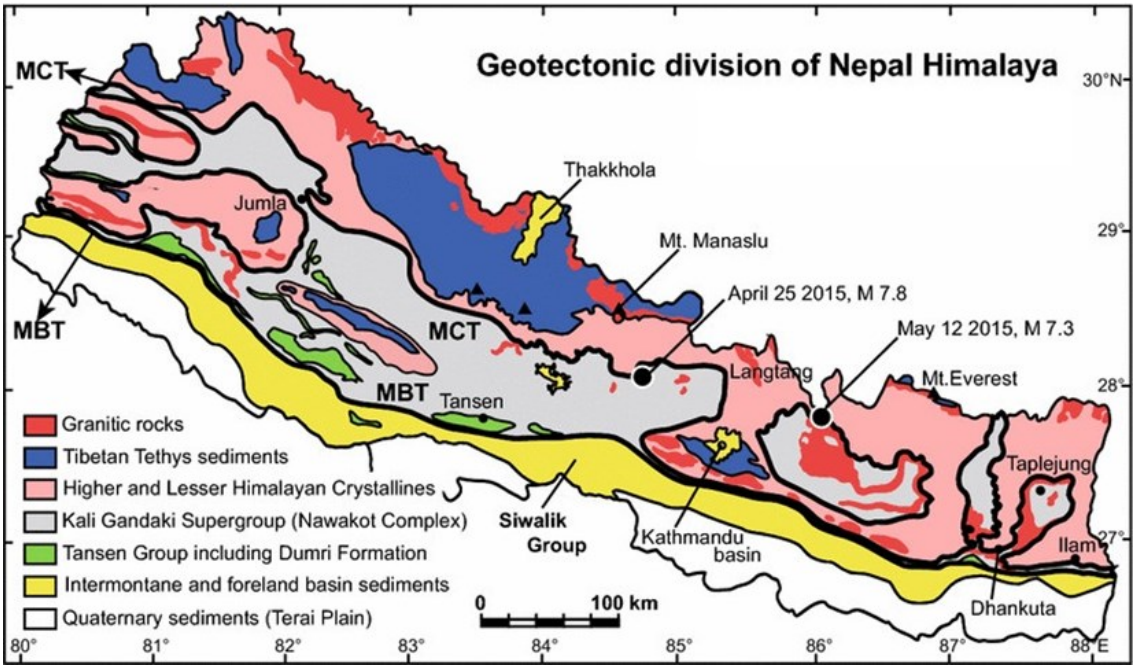

Figure 5 Schematic geological map of Nepal Himalayas with epicenters of 2015 Gorkha Earthquake (Sakai et al., 2016).

2.2.2 Sub-Himalaya (Siwaliks or Churia Group): The Sub-Himalaya (Siwaliks or Churia Group) is found in the southern part of Nepal, represented by the low hills of the Churia Range occupying by foreland basin deposits which are bounded to the north by the MBT and to the south by MFT (Upreti, 1999; Figure 6). One can easily note Sub Himalaya hills in the Himalayan range by noticing the much higher mountains to their north by sharp elevation difference (Medlicott and Blanford, 1879). The Sub-Himalaya of Nepal is made up of 5-6 km thick fluvial sediments of Middle Miocene to Early Pleistocene in age (Dhital, 2015). The sediments are generally layering of mudstone, sandstone, and conglomerate. The Siwalik Group

is divided into three-fold classification as the Lower, Middle, and Upper Siwaliks in ascending order for lithology and increasing grain size (Auden 1935; Hagen, 1969; Dhital, 2015). The Lower Siwalik is comprised of mudstone and sandstone, whereas the Middle Siwalik is constituted by thick-bedded, coarse-grained, "pepper and salt" appearance sandstone. The Upper Siwalik is characterized by the presence of a conglomerate with lenses of muds and sands assimilation with Lesser Himalayan rock matrices (Chaudhary, 1982; Dhital, 2015). Several vertebrate and plant fossils are also reported from the Sub Himalayan rocks of the Nepal Himalaya (Takayasu, 1988; Corvinus and Nanda, 1994; Gurung, 1998).

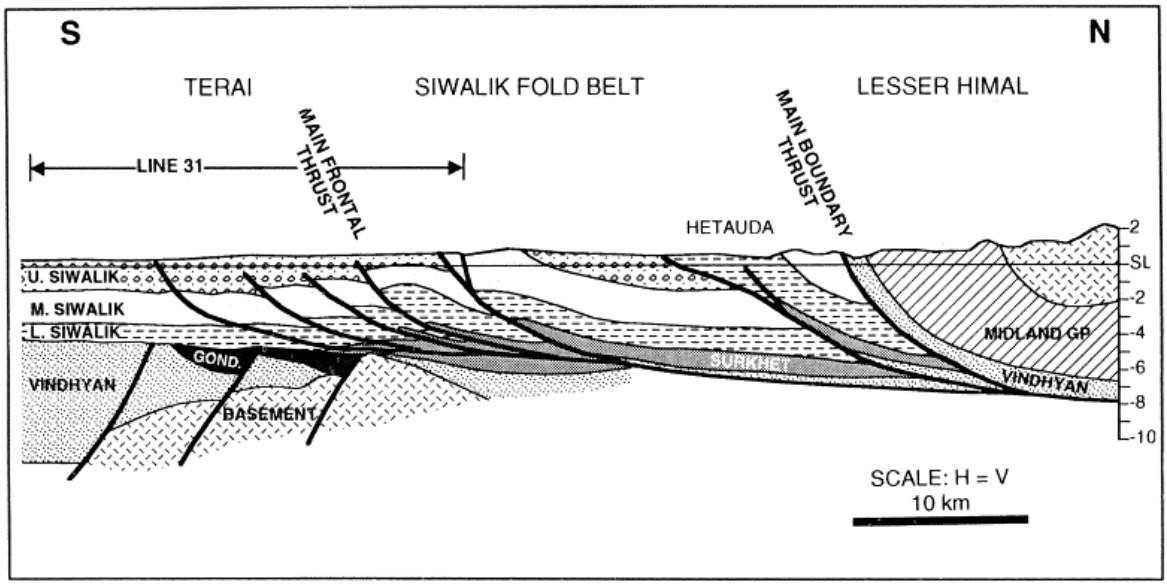

Figure 6 Geotectonic cross-section across Terai, Siwaliks, Lesser Himalaya (Bashyal, 1998).

2.2.3 Lesser Himalaya: The Lesser Himalaya resides in between the Sub-Himalaya (Siwalik Group) in the south and Higher Himalaya in the north which are demarcated by the MBT and MCT respectively (Upreti, 1999). This zone comprises low-grade metasedimentary rock units override with crystalline Nappe and Klippe which allow us to classify non-

metamorphosed to low-grade metamorphic Lesser Himalayan rocks and the rocks of the crystalline nappes of the Lesser Himalayan Zone (Stöcklin and Bhattarai, 1977; Upreti, 1999). The age, stratigraphy, tectonics, and the correlations of the Lesser Himalayan Sequence are difficult to predict due to the unfossiliferous nature of metasedimentary rocks and complicated structure zones (Upreti, 1999). Even if the Lesser Himalayan Sequence is popular for sedimentary and low-grade metamorphic rocks, some granites, augen gneisses, amphibolites, and volcanic rocks are also present in some stratigraphic units (Dhital, 2015). The coal-bearing Lower Gondwana sequence is also found within the Lesser Himalayan sequence of Eastern Nepal (Auden, 1935; Hagen, 1969).

2.2.4 Higher Himalaya: The Higher Himalaya zone is located to the north of MCT, and below the fossiliferous sedimentary sequences of the Tibetan Tethys zone which principally consists of different kinds of gneiss (Upreti, 1999). This zone is geologically as well as morphologically symmetrical and consists of a thick pile of highly metamorphosed rocks. It also consists of migmatites, schists, quartzites, and marbles, alternating with gneiss and intruded by Paleozoic granites and leucogranites (Dhital, 2015) (Figure 7). It is situated between the fossiliferous sedimentary zone (the Tibetan-Tethys Himalaya in the north), separated by STDS, and the Lesser Himalaya, separated by the MCT in the south. Almost 10 km thick succession of the Precambrian crystalline succession of Higher Himalaya is also known as the Tibetan Slab which can be divided into four main units from bottom to top as Kyanite-Sillimanite Gneiss, Pyroxene, Marble and Banded Gneiss, and Augen Gneiss (Lefort, 1975; Lefort, 1975a).

2.2.5 Tibetan-Tethys Himalaya: Tibetan Tethys zone is the northernmost tectonic zone of Nepal Himalaya occupying the region between STDS to the south and Indus-Tsangpo-Suture (ITS) to the north which consists of rock of fossiliferous sedimentary sequences (Upreti, 1999).

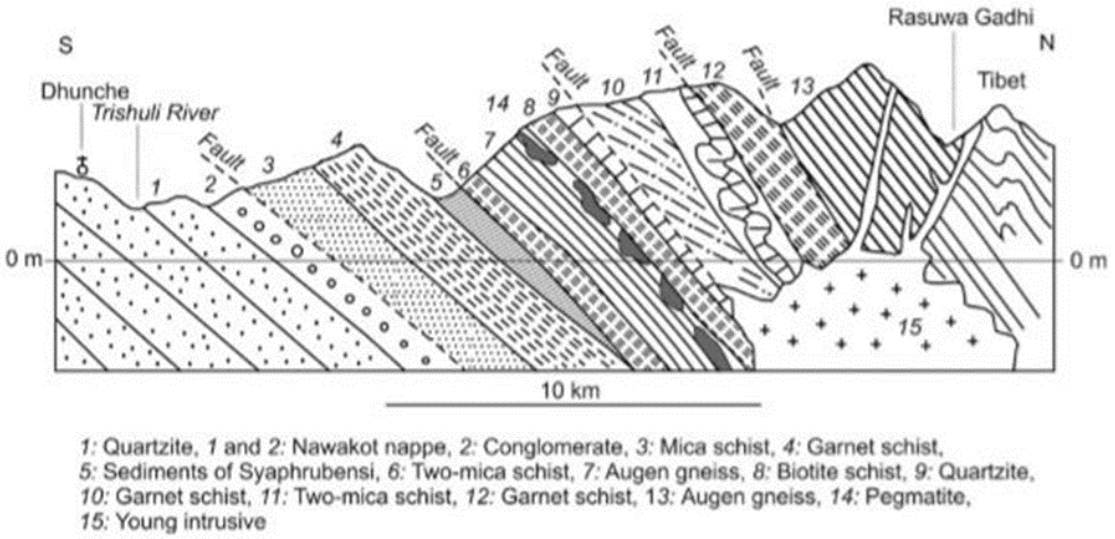

Figure 7 Geological cross-section across the Kathmandu nappes in central Nepal. (Modified from Hagen and Hunger, 1952).

The age of fossiliferous sedimentary sequences of the Tibetan Tethys zone is estimated in the range from Cambrian-Late Cretaceous-Lower Tertiary (Colchen et al., 1986). Most of the high peak mountains of Nepal including Mount Everest are made up of rocks of Tibetan Tethys fossiliferous sequences (Upreti, 1999; Dhital, 2015). In Nepal, these fossiliferous rocks of the Tibetan-Tethys Himalaya are well uncovered in the Dolpa, Thak Khola (Mustang), Manang, Nyj Shang, and Annpurna-Manaslu-Ganesh Himal area (Figure 8).

2.3 Geology of Central Nepal and 2015 Gorkha Earthquake region

Three major fault structures named MFT, MBT, and MCT control the major tectonostratigraphy of central Nepal (Figure 5) where metamorphic grade increases from low to medium along with the MCT (Valdiya 1980; Ahmed et al., 2000). Stöcklin and Bhattarai, (1977) prepared a geological map of central Nepal based on aerial photography in which the area was divided into two complexes named Nawakot Complex and Kathmandu Complex (Table 2). The

autochthonous sequence of the Nawakot Complex and the allochthonous sequences of the Kathmandu Complex is distinguished by the fault named Mahabharat Thrust (MT). The MT is

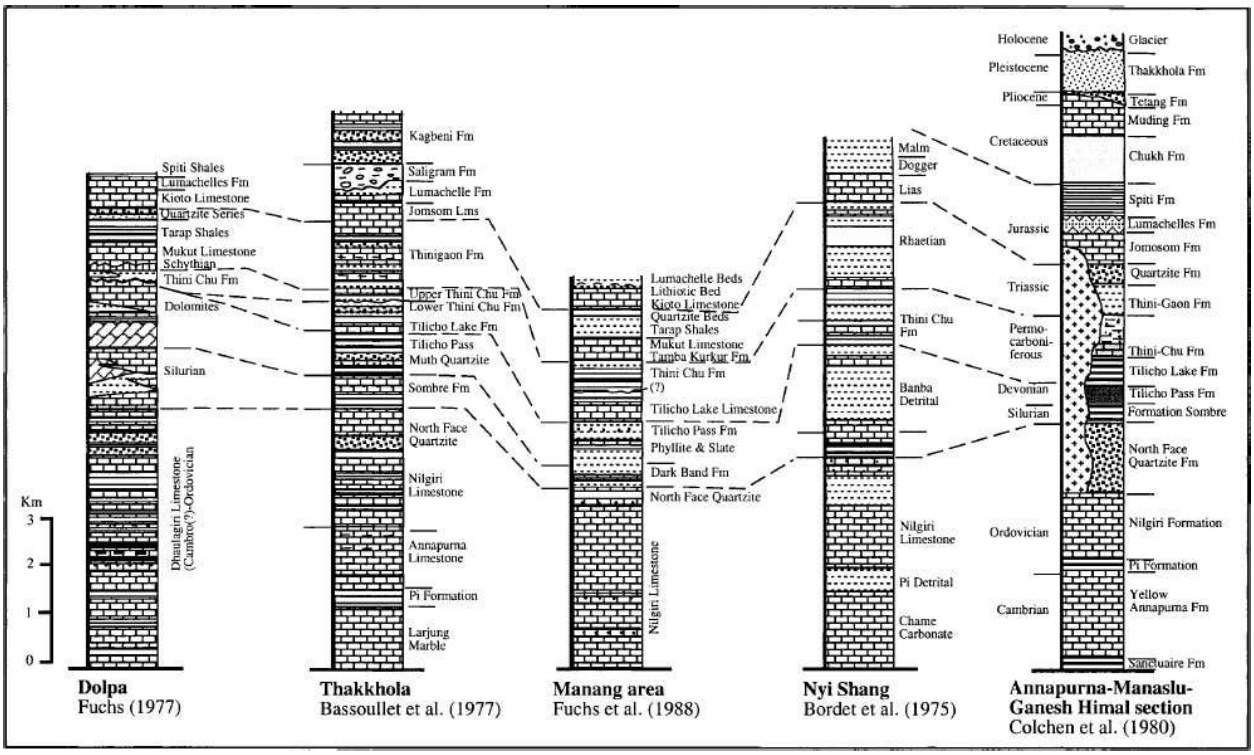

Figure 8 Correlation of Tibetan-Tethys sedimentary formations in different sections of Nepal (Upreti, 1999).

considered as the southward extension of the MCT (Acharya, 2008; Subedi and Acharya, 2016). However, some authors considered it as a separate fault that dragged up the rock of Kathamandu Complex over the Nawakot Complex by forming a nappe structure (Rai et al., 1998; Upreti and Lefort, 1999; Upreti, 1999). The Nawakot Complex is made up of sedimentary to low-grade metamorphic rocks which have been divided into the Lower and the Upper Nawakot Group (Stöcklin and Bhattarai 1977; Stöcklin, 1980). Similarly, the Kathmandu Complex consists of fossiliferous sedimentary rocks to the high-grade metamorphic rock which is also subdivided into Bhimphedi Group and Phulchauki Group. Bhimphedi Group is made up of relatively high-

grade metamorphic rocks whereas the Phulchauki Group consists of unmetamorphic to fossiliferous sedimentary rocks (Stöcklin and Bhattarai, 1977; Stöcklin, 1980).

Table 2 Stratigraphic subdivisions of the Kathmandu and Nawakot Complex (Stöcklin and Bhattarai 1977; Stöcklin, 1980).

Complex	Group	Main Lithology	Age
Kathmandu	Phulchauki	Limestone, slate, calcareous phyllite, metasandstone, and quartzite	Devonian to Precambrian
	Bhimphedi	Marble, schist, quartzite, and garnet schist	Precambrian
Mahabharat Thrust (Southward extension of MCT)			
Nawakot	Upper Nawakot	Phyllite, quartzite, limestone, dolomite, slate, agrellites, and stromatolitic limestone	Early Paleozoic to Precambrian
	Lower Nawakot	Stromatolitic dolomite, phyllite, metasandstone, and quartzite	Precambrian

Rai (2001) has divided the Central Nepal region into three major tectonic units as Lesser Himalaya (LH), Kathmandu Crystalline Nappe (KCN), and Gosaikunda Crystalline Nappe (GCN) (Figure 9). The rock succession of LH is like the rock succession of the Nawakot Complex whereas the rock succession of KCN is like that of the Kathmandu Complex. The GCN lies to the north of the Kathmandu Valley which consists of amphibolite -to granulite – facies high-grade metamorphic rocks (Rai, 2001).

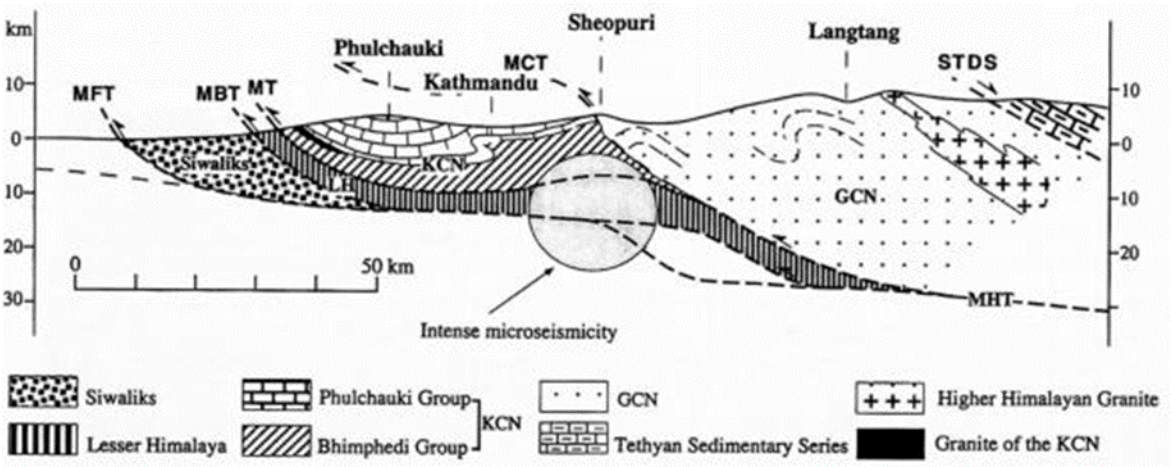

Figure 9 Geological cross-section across Central Nepal with localized intense microseismicity. (Modified after Upreti and Le fort, 1999; Rai, 2001). Where, GCN: Gosaikunda Crystalline Nappe, KCN: Kathmandu Crystalline Nappe, LH: Lesser Himalaya, MBT: Main Boundary Thrust) MCT: Main Central Thrust, MFT: Main Frontal Thrust, MHT: Main Himalayan Thrust, MT: Mahabharat Thrust, and STDS: South Tibetan Detachment System.

The 2015 Gorkha Earthquake Event occurred in the Graphitic Schist unit of Lesser Himalayan Sequence of Jhyallaphat-Barpak-Bhachchek area, Central Nepal (Oli et al.,2019) (Figure 10). The rock succession of this area can be correlated with the rock succession of the Nawakot Complex of Central Nepal (Figure 11). The main earthquake event of 25th April 2015 and the major aftershock event of 12th May 2015 was occurred due to the slip movement on MHT (Hossain et al., 2015). Most of the aftershocks including the mainshock were centered on

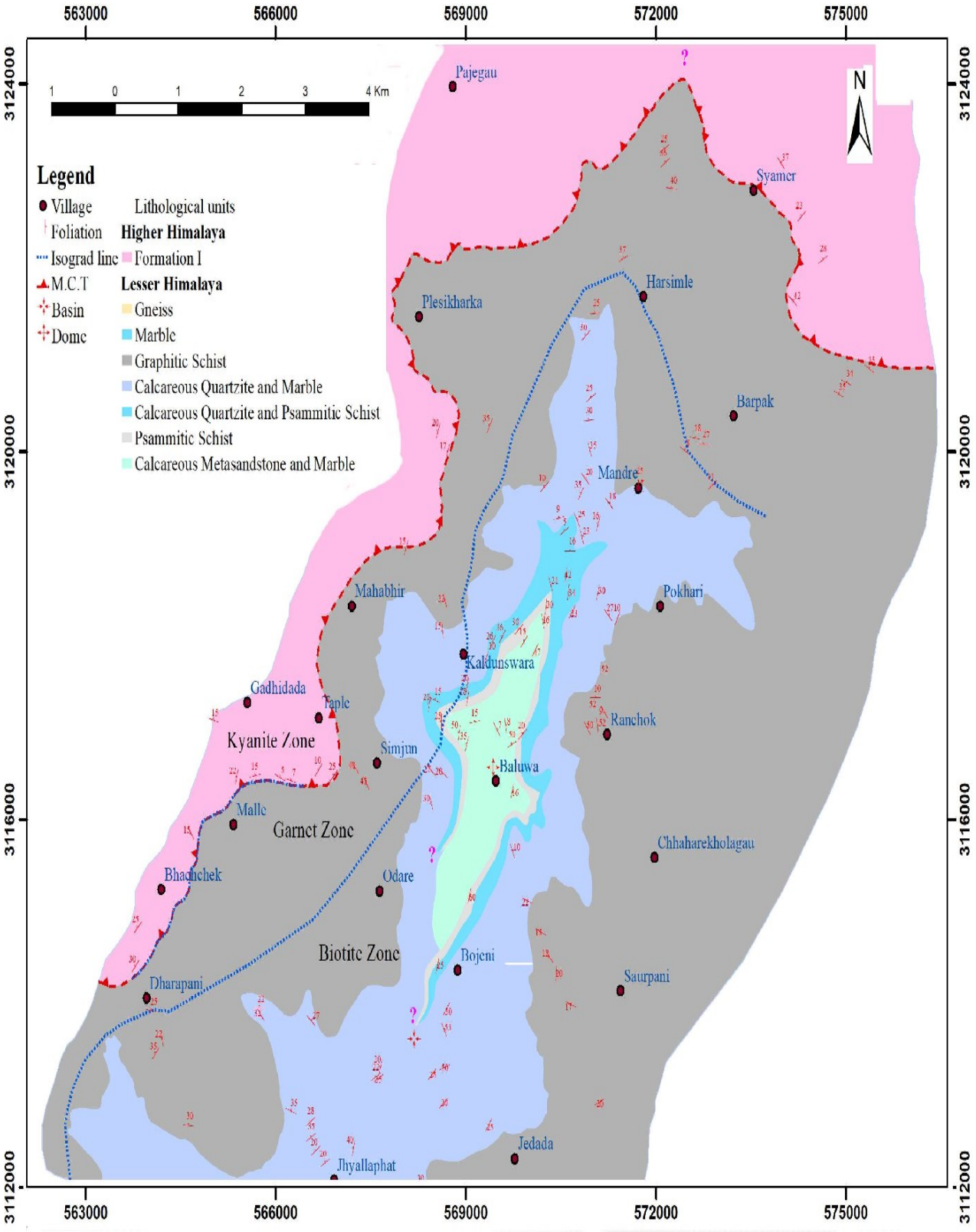

Figure 10 Geological map of Jhyallaphat-Barpak-Bhachchek area with isograde line. The location of the epicenter of the main event is also shown in the rectangular box (Oli et al., 2019).

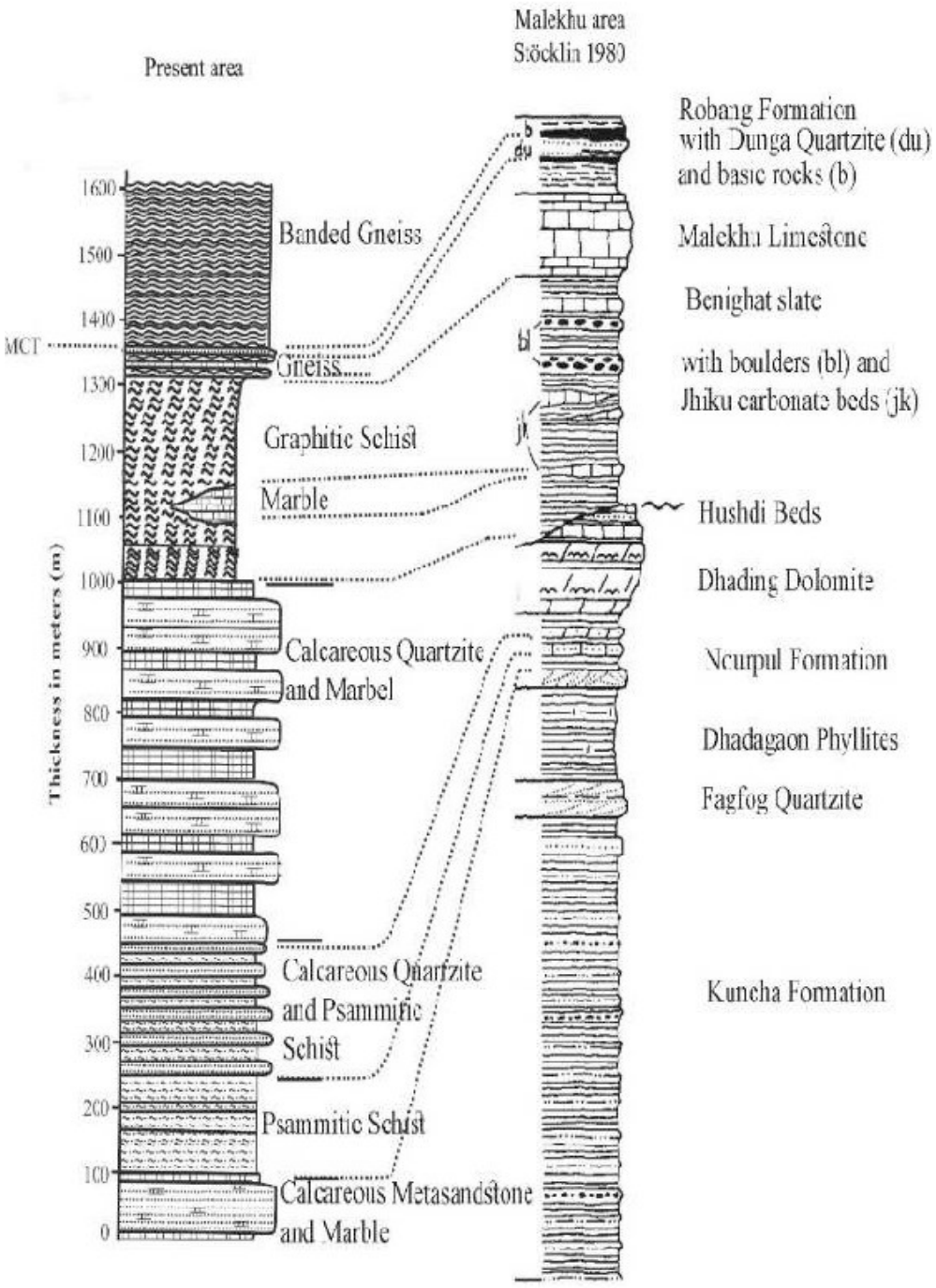

Figure 11 Geological cross-section of rocks from the Jhyallaaphat-Barpak-Bhachchek area correlating with those from Central Nepal Lesser Himalaya (Stöcklin, 1980; Oli et al., 2019).

the Lesser Himalayan sequence and few aftershocks were centered in the Higher Himalayan crystalline Sequence (Figure 12). There were numerous aftershocks. Most of the aftershocks were occupied in low-grade metamorphic rocks (Kargel et al., 2016). Most of the earthquakes

with magnitude range 7.0- 7.8 concentrated in the area consisting of slate, shale, siltstone, sandstone, graphitic schist, and carbonate bands (Figure 13).

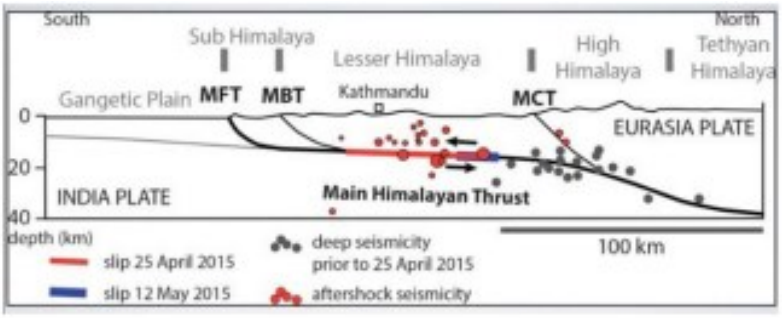

Figure 12 Generalized cross-section of tectonic zonation of the Nepal Himalaya showing the location of foci of the Gorkha Earthquake (Hossain et al., 2015).

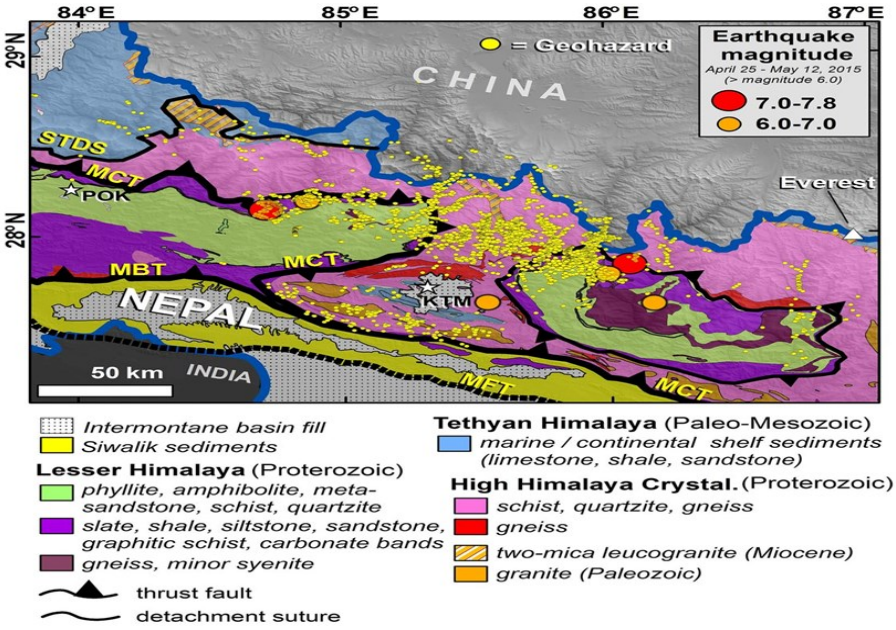

Figure 13 Geological map of central Nepal showing major earthquake epicenters (Kargel et al., 2016). MFT-Main Frontal Thrust, MBT-Main Boundary thrust, MCT-Main Central Thrust, STDS- South Tibetan Detachment System.

CHAPTER-3 PREVIOUS GEOPHYSICAL STUDIES

3.1 Seismic studies in Nepal Himalayan Orogeny

Nábělek et al., (2009) studied the lithospheric structure beneath the Himalayan orogeny in the course of the project Mountain Building (Hi- CLIMB) along a profile in Nepal and Tibet using broadband seismic data (Figure 14). They interpreted receiver functions to outline the edges of crust and upper mantle underneath the Himalaya and southern Tibetan plateau. They also inferred the image of Moho geometry at 40 km underneath the Ganga basin, 50 km underneath Southern Himalayas, and up to 70 km underneath Greater Himalaya. The receiver function implicated the continuation of MHT under the Indian plate and Tibetan plate which has shallow depth under Nepal to mid-crust under southern Tibet (Figure 15).

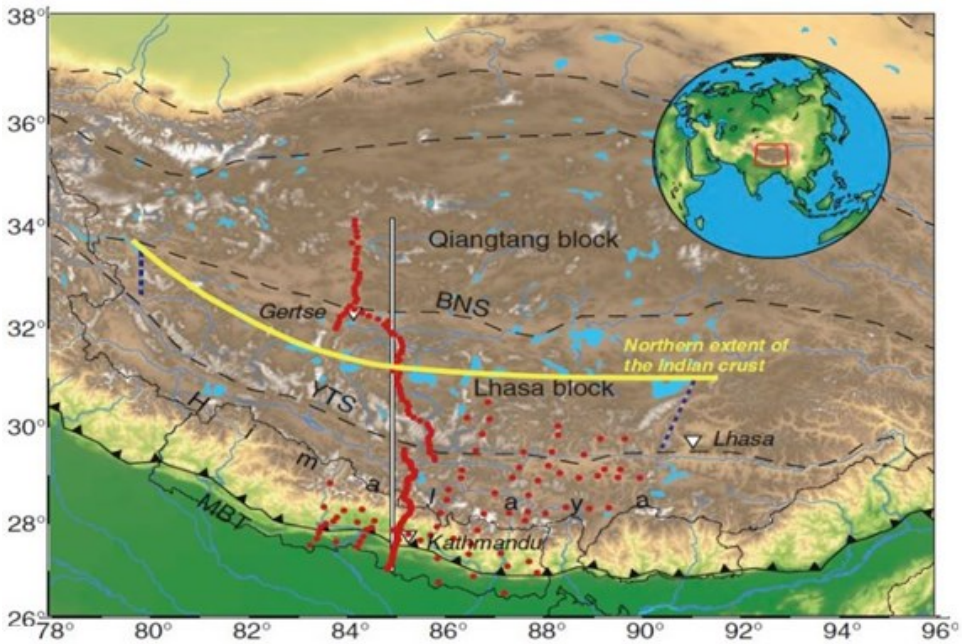

Figure 14 Location map of Hi_CLIMB experiment in Nepal and on the Tibetan Plateau. The small red circles indicate the positions of broadband seismological stations. The cross-section is taken along the profile (White line). (Modified after Nábělek et al., 2009).

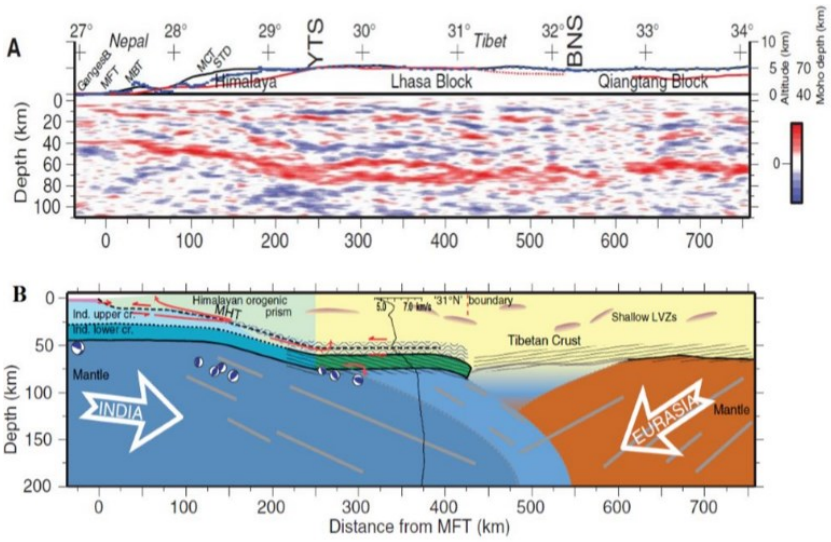

Figure 15 Seismic receiver function image and geological interpretation of Central Himalaya (modified after Nábělek et al., 2009). Figure A is showing the receiver function image with major contrasting boundaries within the lithosphere whereas Figure B is showing geological cross-section interpretation along the India-Asia Collision Zone. The red and blue colors in figure A stands for increasing and decreasing impedance with depth whereas the green color zone in figure B stands for eclogitization of the lower crust. MHT=Main Himalayan Thrust.

3.2 Seismic Studies in Central Nepal and the 2015 Gorkha Earthquake Region

There are major six catastrophic earthquakes (1255 AD,1408 AD,1505 AD,1833 AD, 1934 AD, and 2015 AD) known to occur in the Nepal Himalaya region for 760 years (Thapa et al., 2017). A catalog of the earthquakes with magnitude Ms>4.0 during that period was prepared to analyze their spatial-temporal distribution, which exhibits the uneven scattering of earthquake epicenters with higher earthquake activity in the eastern and western part of Nepal than southern portion (Thapa, 2018). It is also noted that epicenters of most earthquakes are concentrated near the MCT, and the epicenter of few earthquakes reside at some distance from the surface of the MFT and MBT (Figure 16). The latest devastating earthquake occurred on April 25th, 2015 at 7.8 magnitudes which traced the epicenter on the Gorkha district of Central Nepal (Hossain et al., 2016). Most of the aftershocks of these devastating events were centered in the central Nepal region.

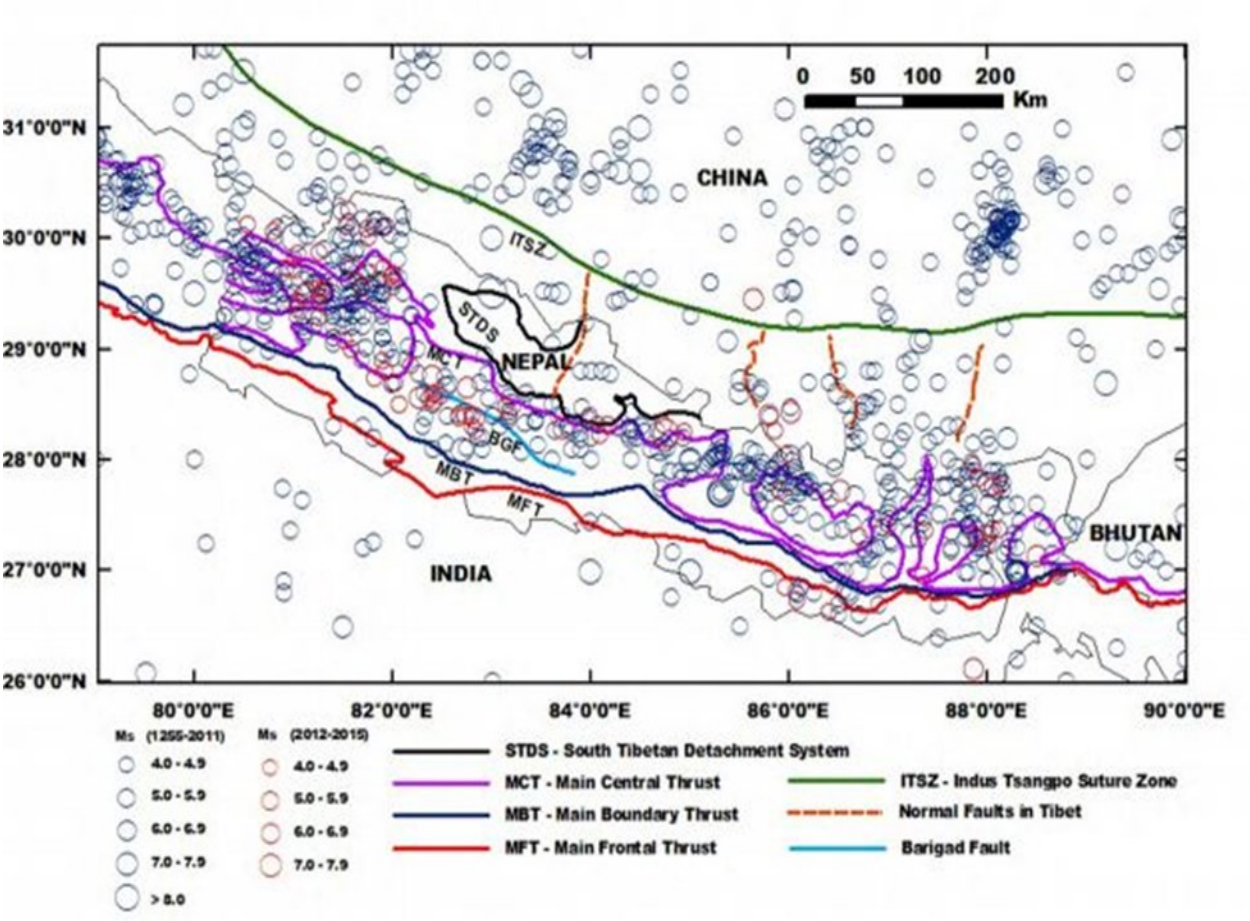

Figure 16 Spatial distribution of earthquakes (Ms≥4.0) occurring in and around Nepal Himalaya between 1255 and 2015. Where ITSZ: Indus-Tsangpo Suture Zone; STDS: South Tibetan Detachment System; MCT: Main Central Thrust; MBT: Main Boundary Thrust; and MFT: Main Frontal Thrust; and BGF: Bari Gad Fault. (Modified after Thapa, 2018).

A slip model of the 2015 Gorkha earthquake was prepared by using the inversion of vector displacement data observed in 13 GPS stations and line-of-sight (LOS) displacement data derived from synthetic aperture radar (SAR) which are tracked from ALOS-2 satellite (Wang et al., 2015; Figure 17). The model suggests that the rupture occurred in a deep part of the MHT where there was little or no slip within 50 km from MFT. The model also provided figures about the shallow dip of the MHT as 7^0.

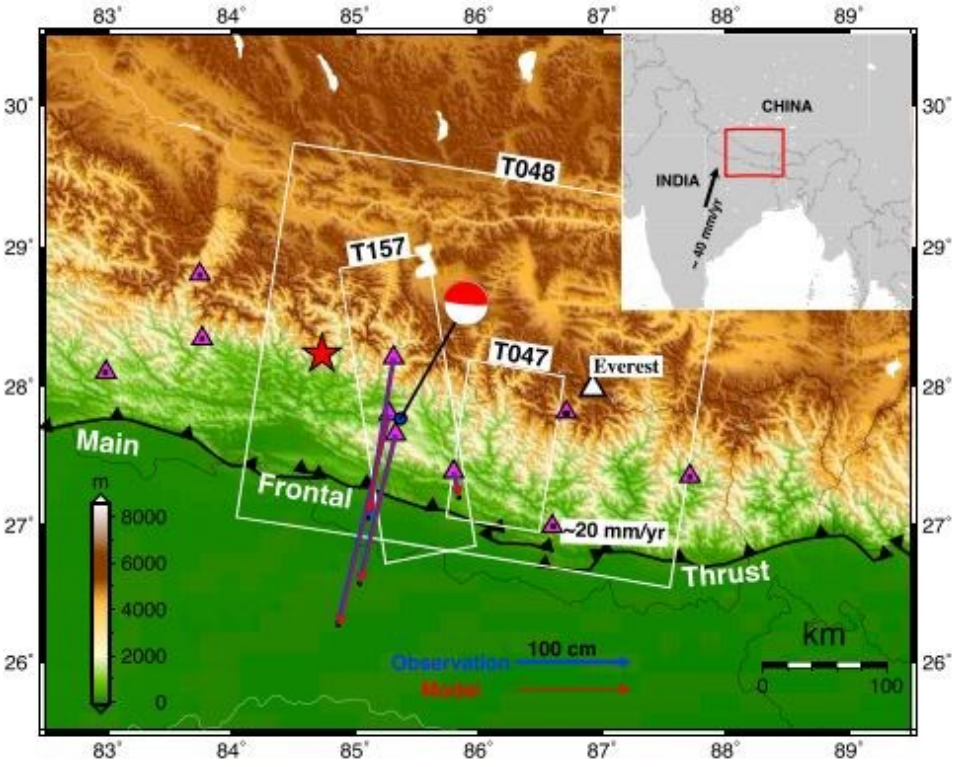

Figure 17 Synthetic aperture radar (SAR) setting to study slip model of the 2015 Gorkha Earthquake (Wang et al., 2015). White boxes show the coverage of ALOS-2 data, the red star denotes the epicenter, magenta triangles represent GPS sites, blue and red arrows represent the observed and modeled horizontal surface displacements at GPS sites, and the thick black line represents the surface trace of the MFT.

The rupture dynamics of the 2015 Gorkha earthquake were explored by computing P-wave spectra of the mainshock and two large aftershocks with an assessment of stress drop and radiated energy (Denolle et al., 2015). It is proposed that a dynamic weakening mechanism administers the runaway rupture pattern of the onset of the mainshock and the largest aftershock. The mainshock relied upon the intersection of two large historical Mw 8+ Himalayan great earthquakes and provided new constraints on rupture propagation through geometric barriers.

The rupture process of the 25 April 2015 Gorkha earthquake was investigated by using kinematic joint inversion of teleseismic waves, strong motion data, high-rate GPS, static GPS, and synthetic aperture radar (SAR) data which concluded that the main slip patch rupture broke

independently at a steady velocity of 3.1- 3.2 km/s which likely comes up with to moderate peak ground acceleration (0.2g) observed in Kathmandu (Gardin et al., 2015). They found that a rupture closer to Kathmandu and presuming more high-frequency emissions might still strike the city in a powerful way than the 2015 Gorkha earthquake.

The lateral variation of the MHT was studied by using seismic waveform recorded by local stations that were in the aftershock zone which included 266 well-located earthquakes, 18 well determined focal mechanisms, and a three-dimensional tomography model to interpret the velocity structure of the MHT at the collision zone (Bai at al., 2019; Figure 18). The lateral variation was known to occur along geological strike, with the Lesser Himalayan ramp having a medium dip on the MHT underneath the mainshock area and flatter and deeper MHT beneath the eastern end of the aftershock zone. It is also disclosed that morphological structures of the MHT controlled the rupture length of the Gorkha Earthquake.

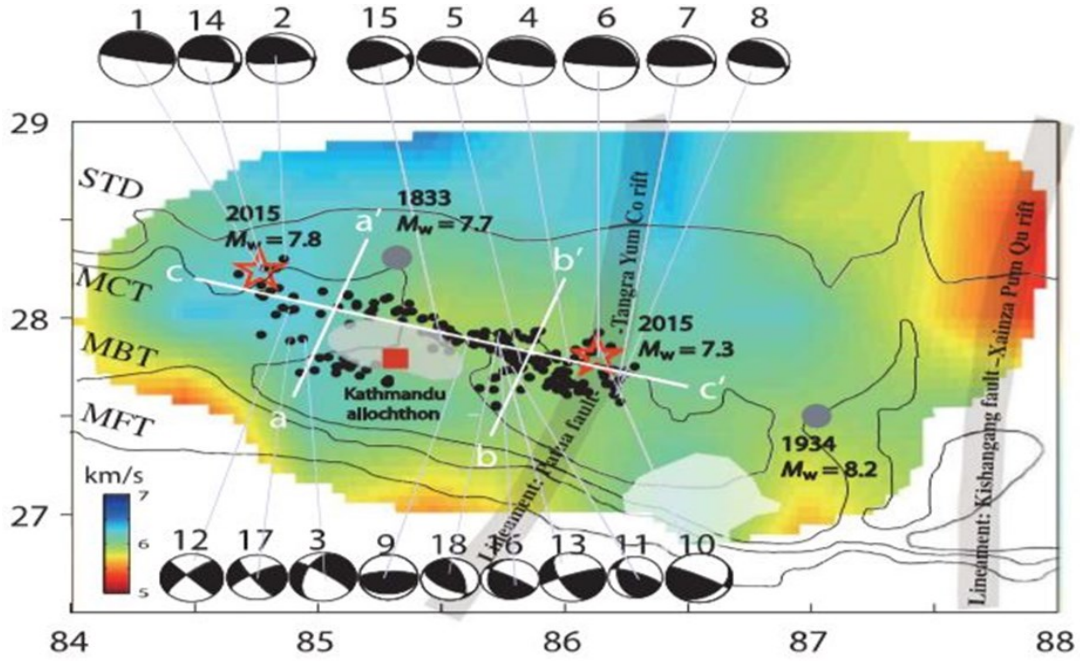

Figure 18 Representation of earthquake relocations, fault plane solutions, and P-wave velocity structures for the MHT surface. (Bai et al., 2019).

The mainshock and aftershocks were recorded by permanent global and regional arrays and by a temporary local broadband array near the China-Nepal border positioned before the 2015 Gorkha mainshock. The total number of 272 earthquakes were located with Mw >3.5 by applying a multiscale double-difference earthquake relocation technique to arrival times of direct and depth phases recorded globally and locally and determined a well-constrained depth of 18.5 km for the mainshock hypocenter which places it on the MHT (Bai et al., 2016).

3.3 Gravity Studies in the 2015 Gorkha Earthquake Region

A gravity base station was established in Nepal during 1981-1984 by the British Military survey as part of the ISGN 1971 reference system and a LaCoste Romberg Model G gravimeter (Manandhar and KC, 2018). The Fundamental Absolute Gravity Stations (FAGS) was established in 1991 March/April at Nagarkot. Besides these stations, a gravity survey was performed during WNTMP (Western Nepal Topographic Mapping Project) and ENTMP (Eastern Nepal Topographic Mapping Project) with observations at GPS stations. Likewise, an airborne gravity survey of Nepal was carried in December 2010 in cooperation between DTU-Space, Survey Department of Nepal, and National Intelligence Agency- NGA USA with goals of providing data for a new national geoid model, which will support GPS surveying and national geodetic infrastructure. The comprehensive accuracy of airborne gravity data collected was 3.3 mGal. The survey had authenticated the official Survey Department height 8848m for Mount Everest within the range of +/- 1m (Manandhar and KC, 2018).

To assess seismic segmentation in a continental collision setting, like Himalaya, arc-parallel topography anomaly (APaTA) and arc-parallel gravity anomaly (APaGA) were computed along the 2500km long Himalayan orogen (Hetényi et al., 2016) in which land gravity

data were taken from many places of Nepal and Bhutan Region (Figure 19). STRM mission at 1 arc- minute resolution was used to obtain topography data within 8km wide radial bins arc perpendicular topography profile. The APaGA manifests largely the deeper orogen structure whereas APaTA manifests relief and the erosional effects within the Himalayan orogeny (Figure 20). Four blocks were demarcated named NE India, Bhutan, Nepal, and India until Dehradun and NW India. The segment boundaries were found unpropagated by the past mega-earthquake in the region which suggests that the boundaries set the limit for potential rupture of the megathrust earthquake. It is recommended to conduct a further geophysical and paleo-seismic study of the area to further characterize the transition between the segment boundaries.

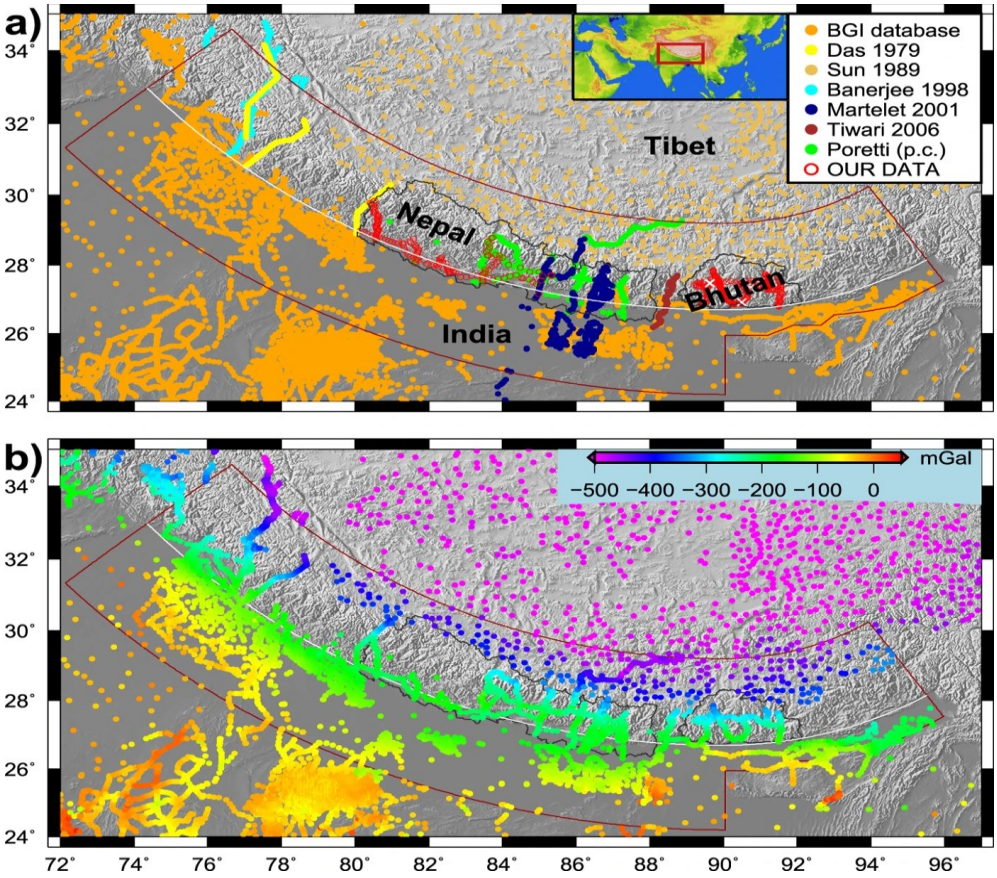

Figure 19 APaTA and APaGAcomputation along The Himalaya (Hetényi et al., 2016). a) Sources of gravity data. b) Bouguer anomaly map of the Himalayas and periphery.

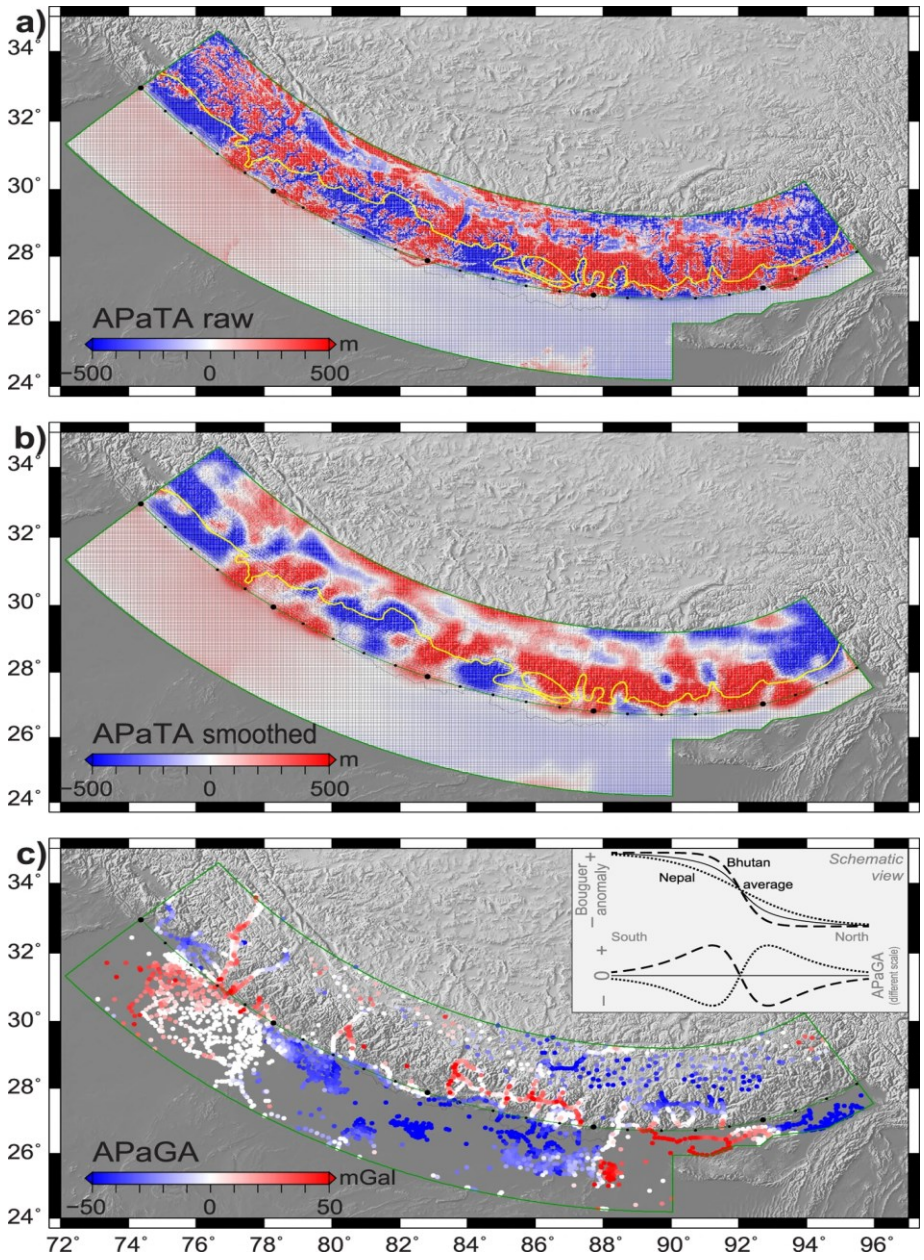

Figure 20 APaTA and APaGA computation results along the Himalayas (Hetényi et al., 2016). (a) APaTA in its raw format. (b) APaTA after smoothing with a 30-km radius circle. (c) APaGA in the study area. Red and blue values represent respectively higher and lower values of topography and gravity whereas the yellow line marks the Main Central Thrust, the boundary between the Lesser and Higher Himalaya formations.

Segmentation of MHT was accessed by using geodetic observation and Bayesian analysis (Zilio et al., 2020) which derive a probabilistic estimation of interseismic coupling along the MHT. Interseismic coupling was assessed from the GPS- derived velocity spacing. The Bayesian

approach was used to derive a probabilistic estimation of the degree of fault locking along the MHT which eventually prepared a Posterior mean coupling model of the Himalayan Megathrust. The model suggests that coupling is high in the front portion of MHT where MFT reaches the surface. Likewise, the coupling is low within the block boundaries where GPS data are less dense (Figure 21). The lateral variation in collision structure was investigated by comparing APTA with the contour line of the coupling and location of the subsurface ridge which suggests that segmentation of the MHT was influenced by inherited tectonic structures involved within the India-Eurasia collision.

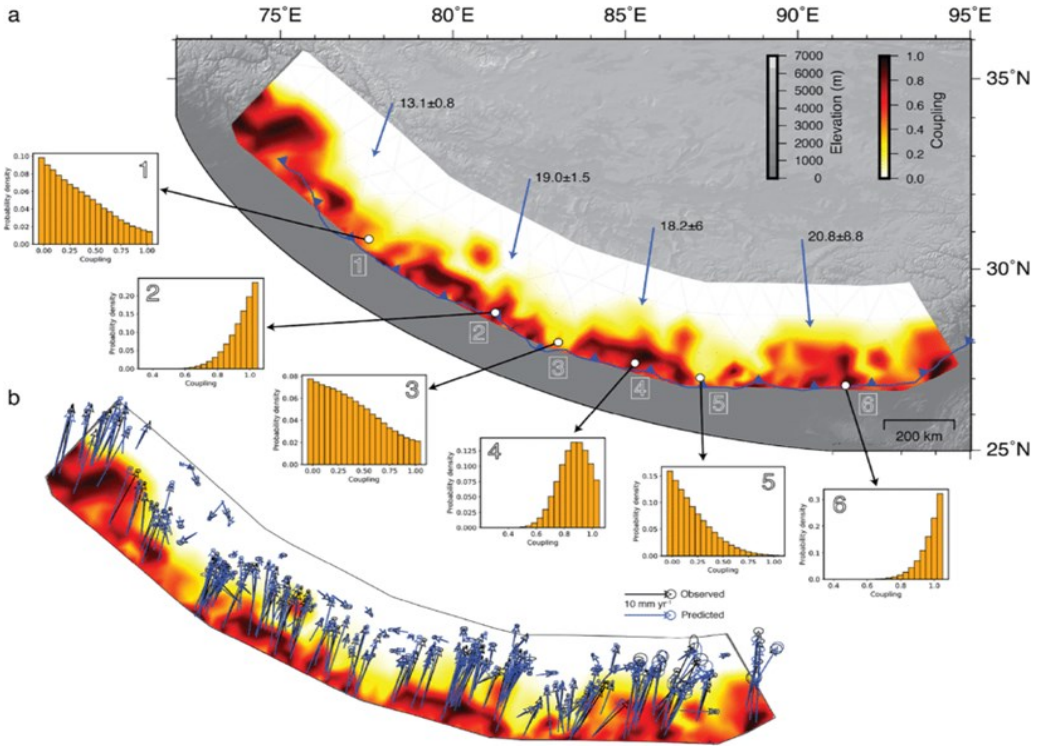

Figure 21 Posterior mean coupling model of the Himalayan megathrust. (a) The resulting posterior mean model with 10% of prediction uncertainties. Where orange bars in each histogram are the marginal probability densities at discrete nodes of the fault model, thin gray lines represent the fault mesh, large blue arrows show the long-term velocities in each region, and the solid blue line shows the surface trace of the Main Frontal Thrust. (b) The same posterior mean model with the GPS displacement where model predictions plotted as black and blue arrows, respectively (Zilio et al., 2020).

In 1970 Japanese Mount Everest Expedition program measured the gravity anomalies of eastern Nepal from different 145-point stations in the form of free-air, Bouguer, Pratt-Hayford, and Airy-Heiskanes anomalies (Kono, 1974). The data were presented in the gravity-elevation format which was grouped into three well-known geo-morphological zonations such as Higher Himalayas, Lower Himalayas, and Foothills. It is noted that Bouguer anomalies do not show any correlation with the elevation whereas Pratt-Hayford and Airy-Heiskanes isostatic anomalies trace a weak positive correlation with elevation. The two-dimensional crustal structure was also shown about the Bouguer gravity anomalies (Figure 22). It is suggested that the Himalayas are

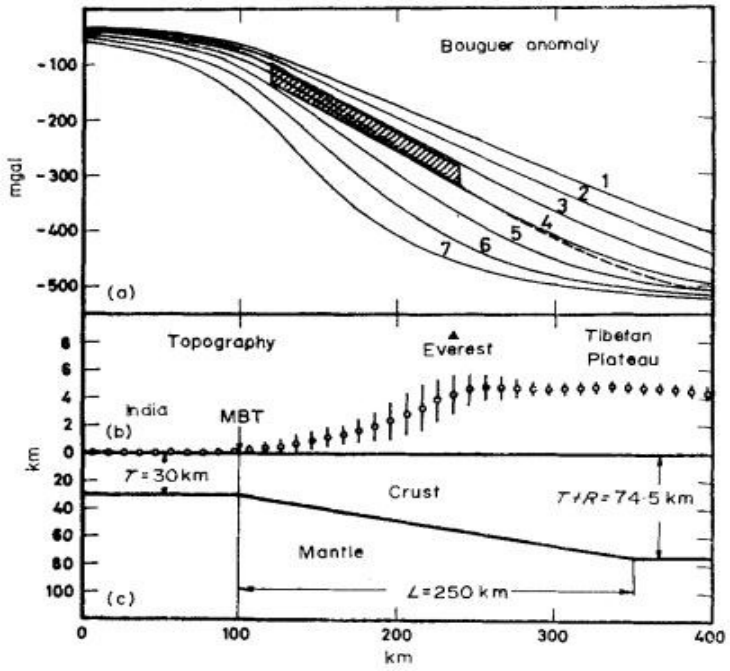

Figure 22 Crustal Structure of Eastern Nepal using Bouguer Gravity Anomalies (Kono, 1974). (a) Observed at sea level for various two-dimensional models. Full lines, for models with Ap = 0.3 g ~m-~, T = 30 km, R = 44.5 km. Curve 1, L = 400 km; 2, 350 km; 3, 300 km; 4, 250 km; 5, 200 km; 6, 150 km; 7, 100 km. Broken line for Ap = 0.6 T = 30 km, R = 22.25 km, L = 250 km. Hatched area shows the Bouguer anomalies in east Nepal in the direction of N lo" E at 95 percent confidence level (+ 2 s.e.). (b) Topographic features of east Nepal and adjacent areas. Circles and bars are the averages and standard error of heights of the 5'x 5' grid points in zones of 20 km wide-stretching in the direction N 100" E. MBT is the Main Boundary Thrust. Vertical exaggeration 10 times. (c) Example of a geophysically plausible model for the crust-mantle structure of the India-Himalayas-Tibet section.

not in isostatic equilibrium which was evidenced by the much thinner crust explored than that expected. This lack of isostatic equilibrium and occurrences of the smooth and oblique substratum was presented as pieces of evidence to explain that the Himalayas are already in the influences of the large-scale tectonic forces.

Mechanical behavior and petrological structure of the lithosphere of the central Nepal collision zone were studied by measuring gravity data at 150 sites along the two profiles perpendicular to Himalaya at the longitude of Kathmandu (Cattin et al., 2001; Figure 23). The

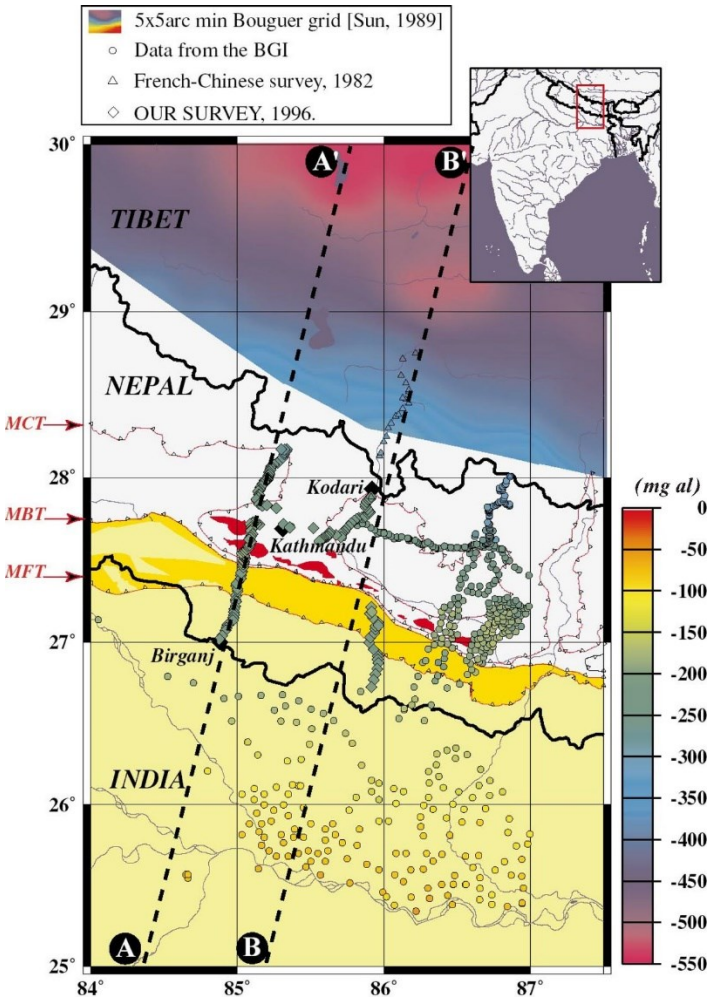

Figure 23 Gravity data observation along with central Nepal (Cattin et al., 2001). The color scale shows complete Bouguer anomalies. Black dashed lines show the locations of profiles AA′ and BB′.

gravity data were used to examine principally two ideas. The first one was about the density of the Himalayan crust which is supposed to be not uniform due to thermal structure. And the second one was mechanical modeling with a realistic temperature and pressure-dependent rheology. The simplified structural sections and complete Bouguer anomaly along the profiles display that Bouguer anomaly diminishes gradually from south to north with the value ranging from -40 to -500 mgal which suggests a steeper gravity gradient (Figure 24). It is also suggested there is locally steeper Moho beneath the high range.

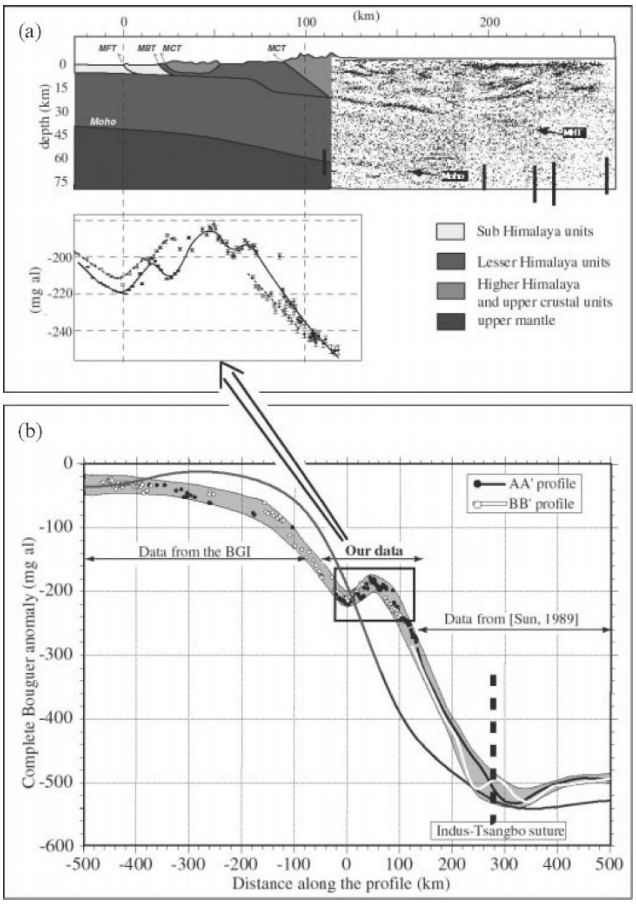

Figure 24 Simplified structural cross-section and complete Bouguer gravity anomaly (Cattin et al., 2001). (a) Simplified structural N18°E section along with profile AA′ across the Himalaya of Central Nepal. (b) Complete Bouguer anomaly along with profiles AA′ and BB′. (Cattin et al., 2001).

The 2-D model of Central Nepal Himalaya which assumes brittle Coulomb failure and non-linear ductile flow was computed from a steady-state thermal Model (Cattin et al., 2001; Figure 25). The modified model predicted equivalent elastic thickness of 40-50 km in the Foreland Basin. At short wavelength, density contrast signal appeared at MBT and MFT, likewise, at intermediate wavelength, hinge and unwrap were observed beneath south Tibet. The negative hinge and positive unwrap features are suggested due to the density contrast resulting from the petrological transformation and eclogitization of the lower crust. It is also clarified that the model was primarily geometrical which cannot be used to examine elastic models.

Chen et.al (2016) used the time-varying gravity data collected during 2011-2013 at four stations out of the hundred gravimetric stations installed by the Crustal Movement Observation Network of China (CMONOC). These four stations were used to determine variations of gravity and to relate them to potential causes of the 2015 Gorkha Earthquake. Since the four gravimetric stations were hundreds of kilometers from the 2015 Nepal earthquake, the researchers modeled the source region as a disk of 150-300 km thick, and gravity changes due to density variation within the disc are assessed by using the popular method of Murthy and Rao (1994). It was summarized that the gravity increased by 22.40 ± 1.11 μGal/yr. These gravity increases may be aligned with strain accretion and possibly mass migration in a broad source region of the 2015 Nepal earthquake. Hubbard et al. (2016) developed a structural cross-section of the central Himalaya, using constraints from surface geology and earthquake analysis of the 2015 Gorkha earthquake. The study extended the cross-section into a 3-D model of the MHT for all of Nepal using surface geology which shows that discrepancies in fault orientation at depth were likely responsible for limiting the size of the Gorkha earthquake. This study also suggested that the detailed studies of the geometry of the convergent systems in the megathrust zone help better

evaluate seismic hazard by identifying constraints on the sizes and locations of future earthquakes.

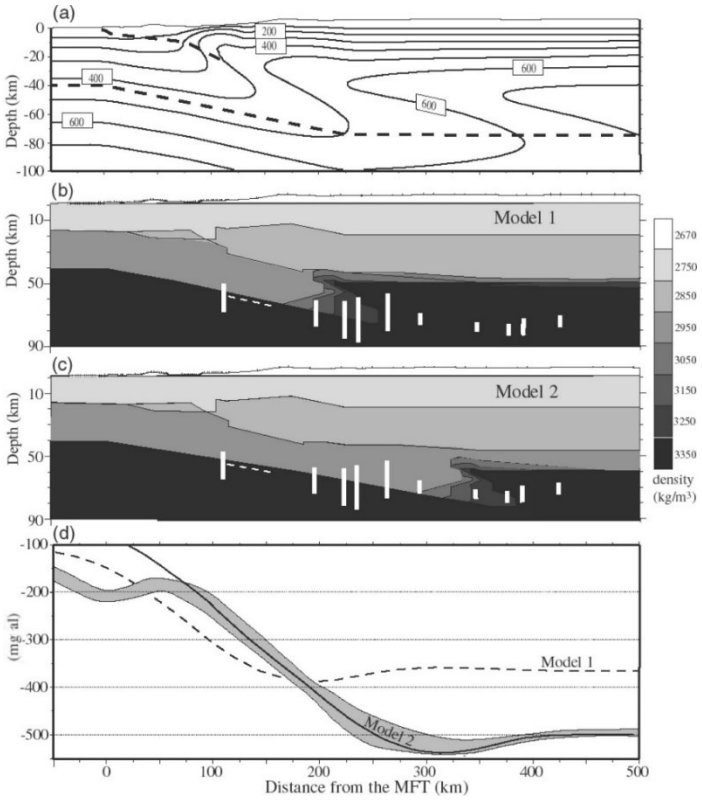

Figure 25 Two-dimensional gravity model of Central Nepal (Cattin et al., 2001). (a) Steady-state temperature field derived from a 2-D computation in which the kinematics of thrust faulting and erosion at the surface is prescribed (b) Density model deduced from a steady-state thermo-petrological model. (c) A modified model assuming that eclogitization is delayed by 6.5–8.5Myr. (d)The corresponding anomaly model more consistent with the gravity data.

CHAPTER-4 DATA COLLECTION

4.1 Gravity Data Collection

The gravity data were acquired from the U.S. National Geospatial and Imaging Agency (formerly the Defense Mapping Agency). The airborne gravity survey was carried out in December 2010 by the Danish National Space Institute, Technical University of Denmark (DTU-Space) in cooperation with the Nepal Survey department and US National Geospatial-Intelligence Agency (NGA) to provide data for a new national geoid model as well as to provide data for future global gravity field models (Forsberg et al., 2014). The airborne gravity survey of the entire country was covered using a COWI Beech King Air Aircraft for 57 flight hours with 6 nm spacing and 3.75 to 9.85 km survey height (Figure 26). The varying in survey heights was due to the changing terrain elevation from south to north; low lying flat land on the southern portion and higher peaks on the northern portion. For the gravity measurements, a Lacoste and Romberg S-type gravimeter running with ultras control systems was mounted in the aircraft which works together with several GPS receivers onboard. Gravity data are missing in the border regions of the country due to the restriction of flight of aircraft in the border region.

A GPS reference station used the station in KATHMANDU J (Airport) and was tied to KATHMANDU AGB-2 (Survey Department), and the absolute gravity station (Nagarkot). The gravity results were based solely on data from LaCoste and Romberg Gravimeter. Free-air gravity anomalies at aircraft level are obtained from:

$$\Delta g = f_z - f_{z0} - h'' + \delta g_{eotvos} + \delta g_{tilt} + g_0 - \gamma_0 - (\partial\gamma/\partial h\,(h - N) + (\partial^2\gamma/\partial h^2\,(h - N)^2)$$

Where, Δg is free air gravity anomaly, f_z is Gravimeter reading, f_{z0} is apron based gravimeter reading, δg_{tilt} is tilt correction value, g_0 is apron gravity value, δg_{eotvos} is eotvos correction value,

γ_0 is Normal gravity value, N is geoid undulation, h is GPS ellipsoidal height, and h" is GPS vertical acceleration.

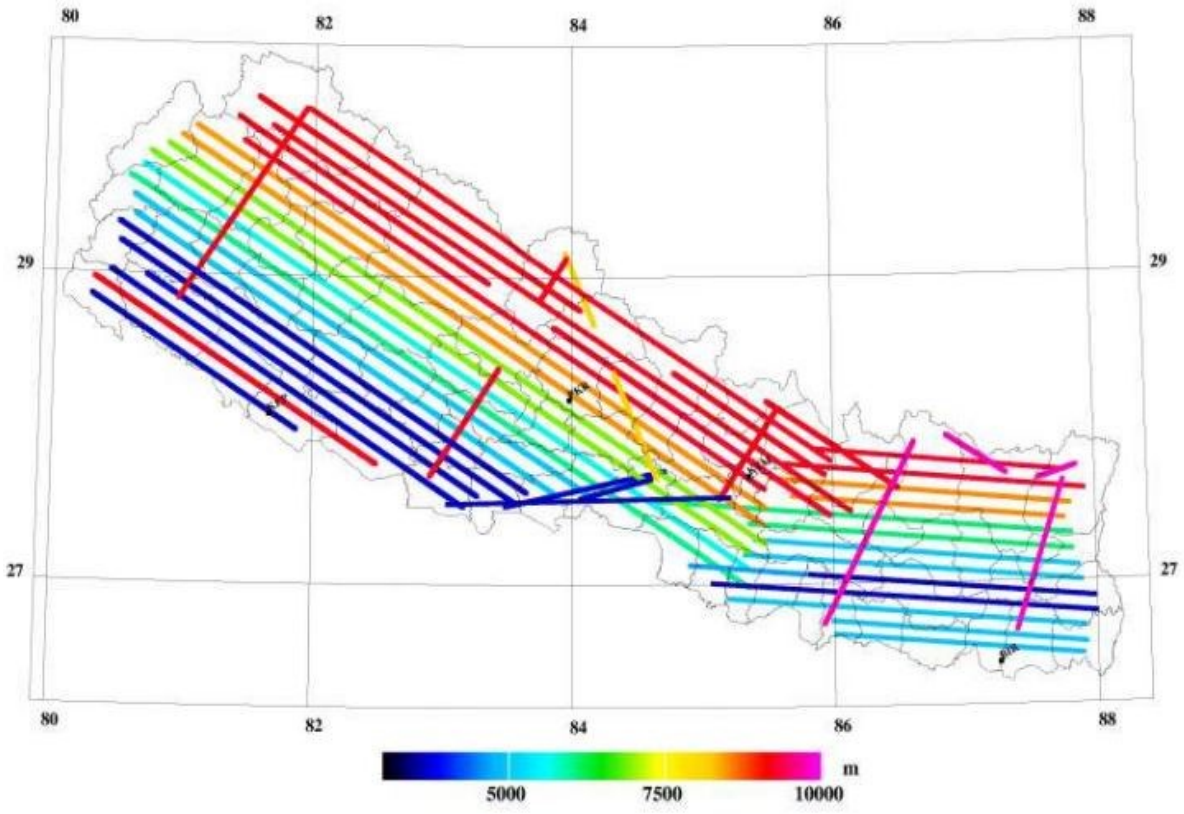

Figure 26 Flight tracks of the Nepal airborne gravity survey. Colors show the flight altitude, ranging from 3700 to 9850m (Forsberg et al., 2014).

The final data set was composed of 104 intersections with a 12.4 mGal RMS gravity. The RMS value was first reduced to 7.3 mGal and then to 4.6 mGal with the help of downward continuation. The overall survey accuracy is estimated to be 3.3 mGal RMS with some minimal errors due to uncertainty in gravimeter scale factors. As a result of this survey, a new geoid of Nepal was computed using Fourier Methods on the downward continuation of airborne data from height to terrain level.

4.2 Land Gravity Data

The first land gravity base was established in 1981-84 by British Military survey using ISGN 1971 gravity reference system and Lacoste and Romberg Model-G gravimeter (Manandhar and KC, 2018). The gravity reference station was established as KATHMANDU J in Tribhuvan International Airport, Kathmandu where gravity reading was obtained as KATHMANDU J = 978661.22+ -0.047 mGal. Likewise, the gravity reference station (FGS) was established on Nagarkot where gravity reading was noted as FGS= 978494834.7+ -6.7 microgal. The gravity data were collected in three main gravity surveys as first-order gravity network of Nepal, absolute gravity observation, and Western Nepal Topographic Mapping Project (WNTP), and Eastern Nepal Topographic Mapping Project (ENTP). All together 375 gravity stations were established, and 1114 gravity points were collected (Figure 27).

4.3 Combined Gravity Dataset

Land gravity data and airborne gravity data of the area were merged. Each gravity station consists of latitude, longitude, Bouguer gravity, outer zone terrain, inner zone terrain correction, elevation in meters, and observed gravity.

4.4 Gravity Data Processing

The gravimeter reading is in gravity meter units and not in mGal. The meter reading on the gravimeter must be multiplied by a meter constant to calibrate. Then the local gravity base stations were rearranged with respect to an absolute local gravity value using the absolute gravity reading that was recorded in the KATHMANDU J. base station. After this, the adjustment was applied to all the gravity stations. These steps assured that the gravity data were adjusted for

instrumental drift correction and latitude correction. The main goal of gravity data processing is to ease data interpretation by removing those gravitational effects which are not related to density variation due to subsurface structures. To do these additional corrections were made.

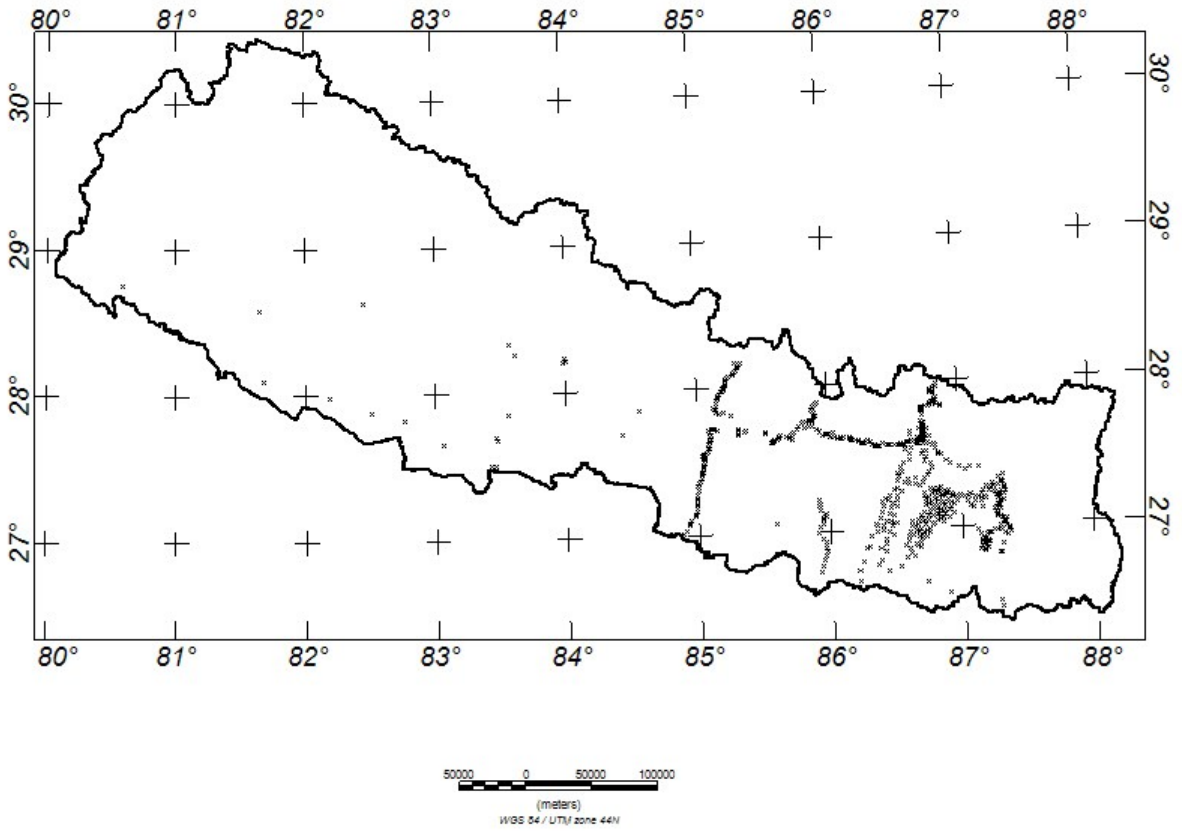

Figure 27 Land gravity data of Nepal. The crosse plus (+) sign represents the land gravity measurement points and color represents the range of gravity value.

Gravity data depends on the elevation of the observed location. There is an inverse correlation between elevation and gravity (Figure 28). The Nepal Himalaya has a high variation in elevation from south to north (Figure 29). Free air anomaly gravity anomalies were calculated and added to the gravity data to account for the gravity variation due to changes in gravity. The

Free Air correction assumes that there is only air that fills the space between the station and datum without any mass, but there is a mass of earth materials. To account for the mass of rock that rests above the datum, a Bouguer gravity correction was made. A Bouguer gravity correction was performed by calculating a Bouguer gravity anomaly using a reference density of 2.67g/cm3 and subtracting this value from the observed gravity value.

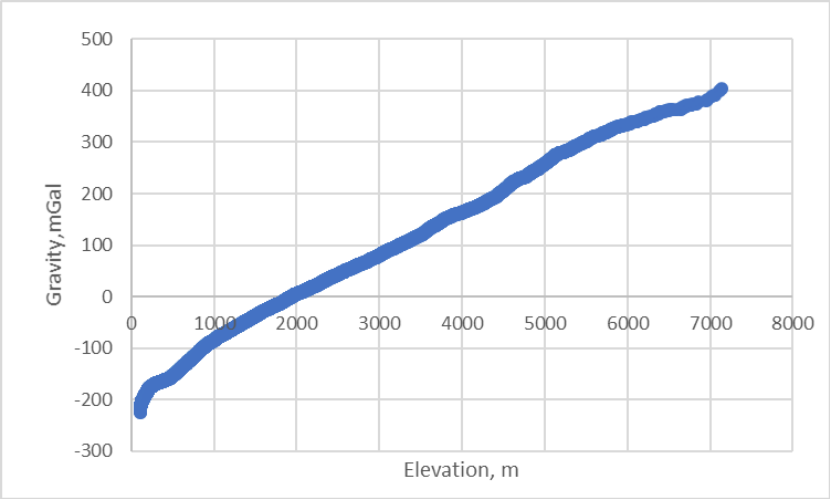

Figure 28 Graph showing Gravity Vs Elevation in Nepal Himalaya. The gravity value is decreasing with increasing elevation.

In a rugged terrain area such as the Himalayan region of Nepal, the adjustment of a flat horizontal landmass between the station and the datum is a difficult task. In this scenario, the gravity measurement registered by the gravimeter is affected by either the upward attraction of the adjacent hills or the lack of mass in adjacent valleys. So, a terrain correction is required for each station. To perform terrain correction, Geo-Soft Oasis Montaj program was used in which the 10 m Advanced Land Observatory Satellite (ALOS) digital elevation model (DEM) was used as local terrain grid, 90 m Shuttle Radar Topography Mission (SRTM) DEM as a regional grid,

and 2.67 g/cm3 as the density of the rock. The terrain correction values thus obtained were added to gravity data to acquire a complete Bouguer gravity anomaly.

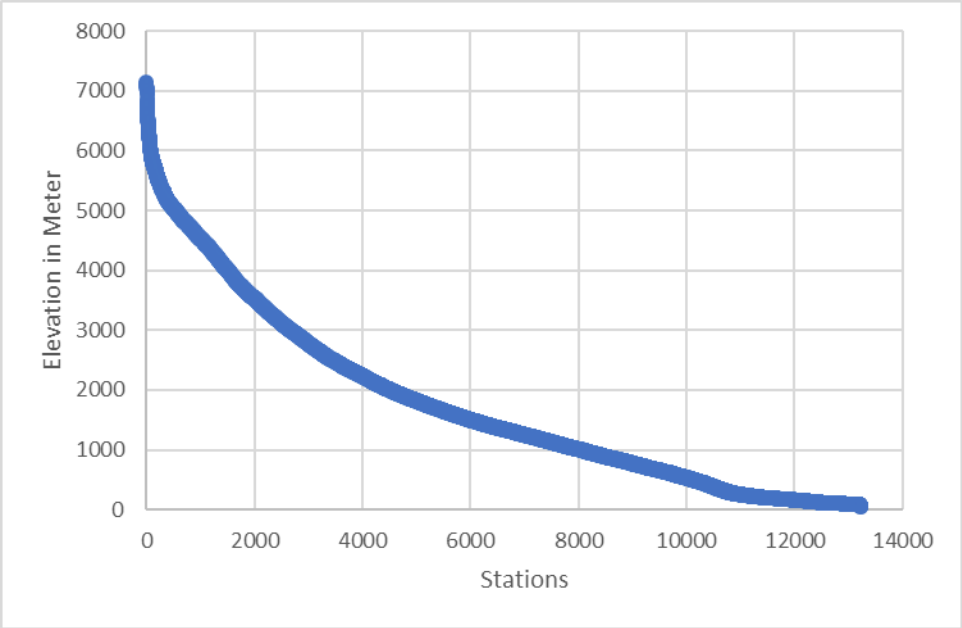

Figure 29 Elevation graph of Nepal Himalaya in each gravity station. A high variation of elevation can be seen in the graph.

CHAPTER-5 GRAVITY DATA ANALYSIS

5.1 Bouguer Gravity Anomaly Map

The complete Bouguer gravity anomaly data were gridded at a spacing of 2 km using the minimum curvature method and to create a Complete Bouguer gravity anomaly map (Figure 30).

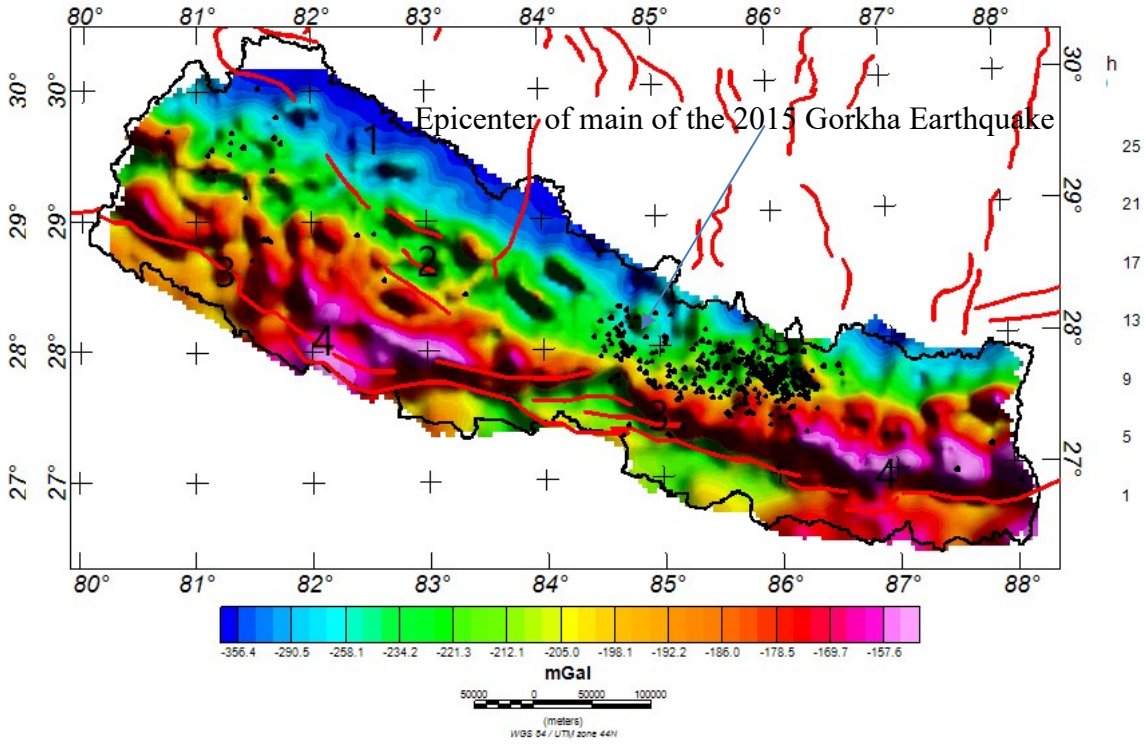

Figure 30 Complete Bouguer gravity anomaly map of the Nepal Himalaya with major fault line in red. The map shows a decreasing complete Bouguer gravity anomaly value towards the north. The black triangular shapes represent the earthquake epicenters. The anomaly layer is grouped into 4 layers from 1 to 4.

The Bouguer gravity anomaly observations in the Nepal Himalaya show a large-amplitude gravity minimum with decreasing values towards the north. The region of lower gravity values

corresponds to the higher elevated areas and the region of higher gravity values to the lower elevated areas. A minimum of -437mGal was found in the northern region of the study area and a maximum value of -45 mGal was recorded in the southern region of the area. The inverse relation between the gravity anomaly and the elevation can be seen in Figure 31. The inverse relation between gravity and elevation is principally caused by a regional mass deficiency at depth due to a lack of isostatic compensation (Simpson et al., 1986).

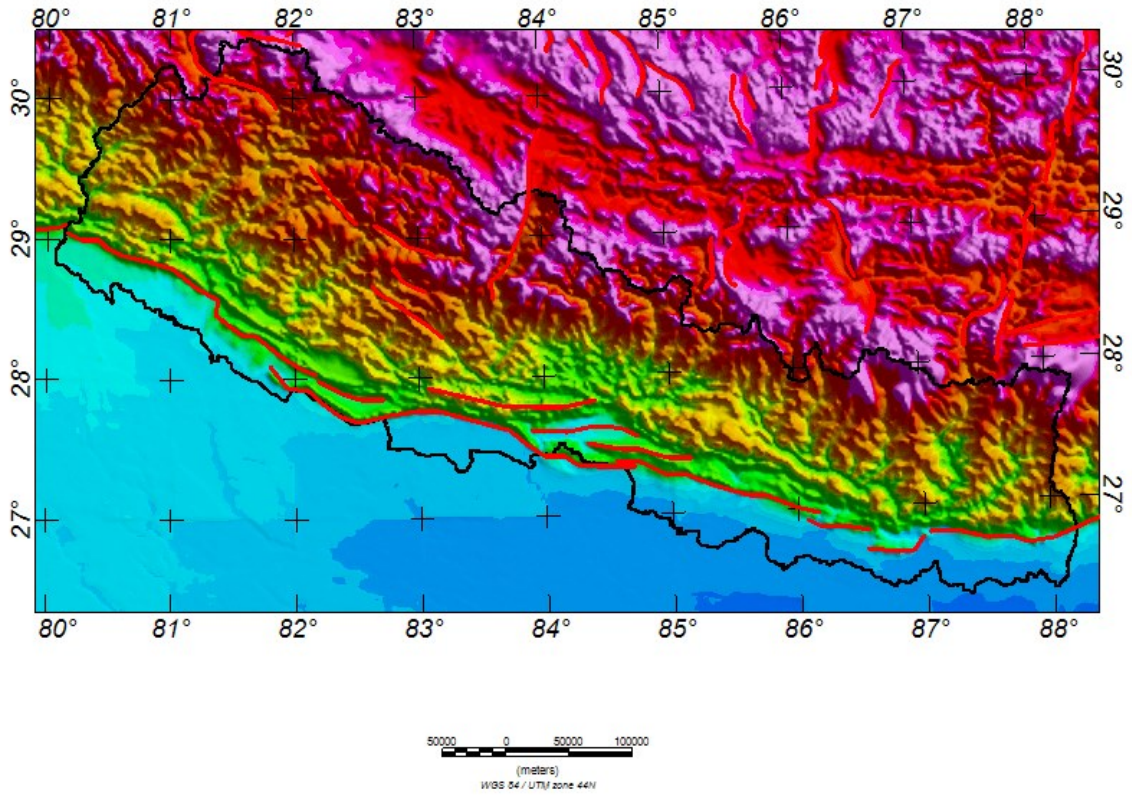

Figure 31 Elevation map of Nepal overlain with major faults (red). The elevation values gradually increase towards the north, the same as the complete Bouguer gravity anomalies.

The complete Bouguer gravity anomalies in general are associated with the regional scale density variation rather than the near-surface lateral density variation. Therefore, the distinct

demarcation between the different tectonostratigraphic boundaries of the area cannot be revealed by only the gravity anomalies. However, the correlation between the geological map and the complete Bouguer gravity anomaly map can give a better clue. The correlation between the Bouguer gravity anomaly and the geological units can be observed in Figure 30 and Figure 32.

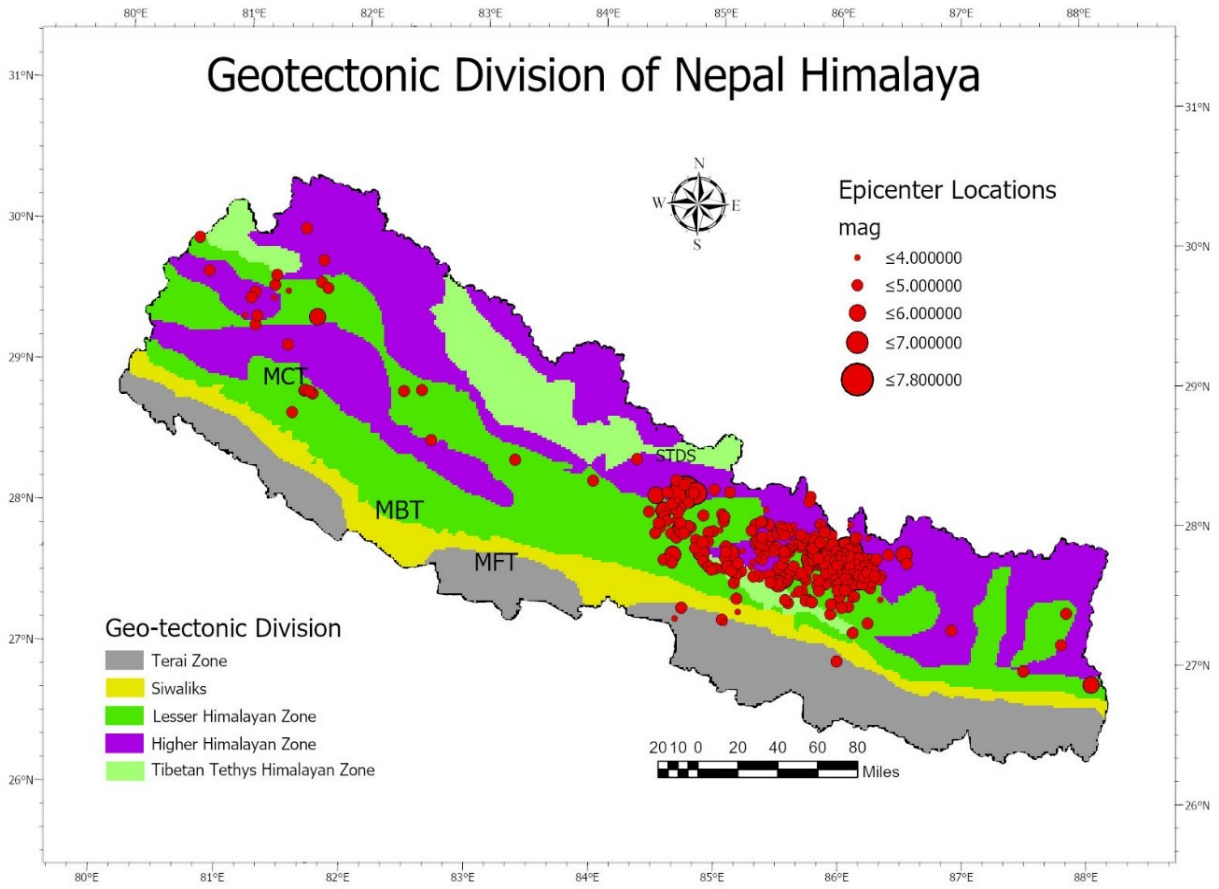

Figure 32 Simplified geological map of the Nepal Himalaya (modified after Dhakal, 2015). The red circles represent the epicenters of the mainshock and aftershocks of the 2015 Gorkha Earthquake. MFT-Main Frontal Thrust, MBT-Main Boundary Thrust, MCT- Main Central Thrust, and STDS-South Tibetan Detachment System.

The gravity value decreases towards the Tibetan Tethyan zone and increases towards the Siwalik zone. In general, the complete Bouguer gravity anomaly in the Siwalik zone has relatively higher

values than other regions, ranging on average between -169 mGal to -155 mGal. The comparison between the elevation, geology, and complete Bouguer gravity anomalies indicates that the complete Bouguer gravity anomaly values decrease towards the north due to crustal thickening. One can notice that most of the fault boundaries are co-linear with the gravity maxima and minima boundaries. The main event of the 2015 Gorkha earthquake also lies in the region separating two areas of gravity minima, which suggests a variation of crustal structure within the region. Likewise, most of the aftershocks locate in the region separating gravity maxima and minima.

5.2 Qualitative Map Analysis Techniques

The combined effect of density variations at depth causes local and regional scale gravity anomalies as can be seen on the complete Bouguer gravity anomaly map (Figure 30). Most of the fault lines are perfectly co-linear with the gravity boundaries and a few are not. The anomalies which are lined up with geological and structural features are easier to understand than those that do not. In this context, different computational methods can be employed depending on the features or size of the anomalies, including wavelength filtering that incorporates band-pass and high-pass filtering (Peeples et al., 1986), horizontal derivatives (Blakely and Simpson, 1986), isostatic gravity residual anomalies (Simpson et al., 1986), and Euler's deconvolution (Reid et al., 1990). These computational methods help us interpret gravity anomalies concerning geological features. However, one must be careful about the spurious anomalies that can occur because of numerical manipulation (Scott et al., 1987).

5.2.1 Isostatic Residual Gravity Anomaly Map: In general, isostatic gravity corrections are based on simple geologic models that represent general earth crustal structure (Simpson et

al., 1986). If the compensating masses are not adjusted during the Bouguer gravity processing, especially in the case of the mountainous region, the resulting Bouguer gravity anomaly will be lower. Zhang et al. (2010) and He et al. (2014) described the isostatic gravity anomalies as the effects of crustal thickening, density variations in the crust structural zoning, and crustal movement which can be used to relate regional geologic structure and earthquake activity. Lingshun et al. (1995) advocated Pratt's Hypothesis for calculating isostatic gravity anomalies in and around the Tibetan plate. Furthermore, the Airy-Heiskanen hypothesis was validated by Simpson et al. (1986) to calculate isostatic gravity anomalies within the United States. Isostatic gravity anomalies can be discerned as the difference between the observed gravity field and the field produced by an isostatically balanced lithosphere. The opposite correlation between a Bouguer gravity anomaly and the topography presented in Figure 28 also highlights the necessity of the isostatic correction to understand the structure beneath the Nepal Himalaya.

To calculate the isostatic gravity anomalies, sea level was assumed as a datum and the depth of compensating material below the datum was calculated using topographic grids. At each grid point, the isostatic regional gravity anomaly was calculated according to the Airy isostatic model. The SRTM DEM (30 m spatial resolution) topographic grid, the thickness of compensating depth, crustal density, and Moho density were the parameters used in the model to calculate the isostatic regional gravity anomalies. Several compensating depths were used between 50-70 km and a depth of 50 km was selected for a model. Likewise, the crustal and Moho densities were considered as 2.67g/cm^3 and 3.3g/cm^3, respectively. The regional isostatic grid was calculated and was subtracted from the complete Bouguer gravity field to produce an isostatic residual gravity anomaly map exhibited in Figure 33.

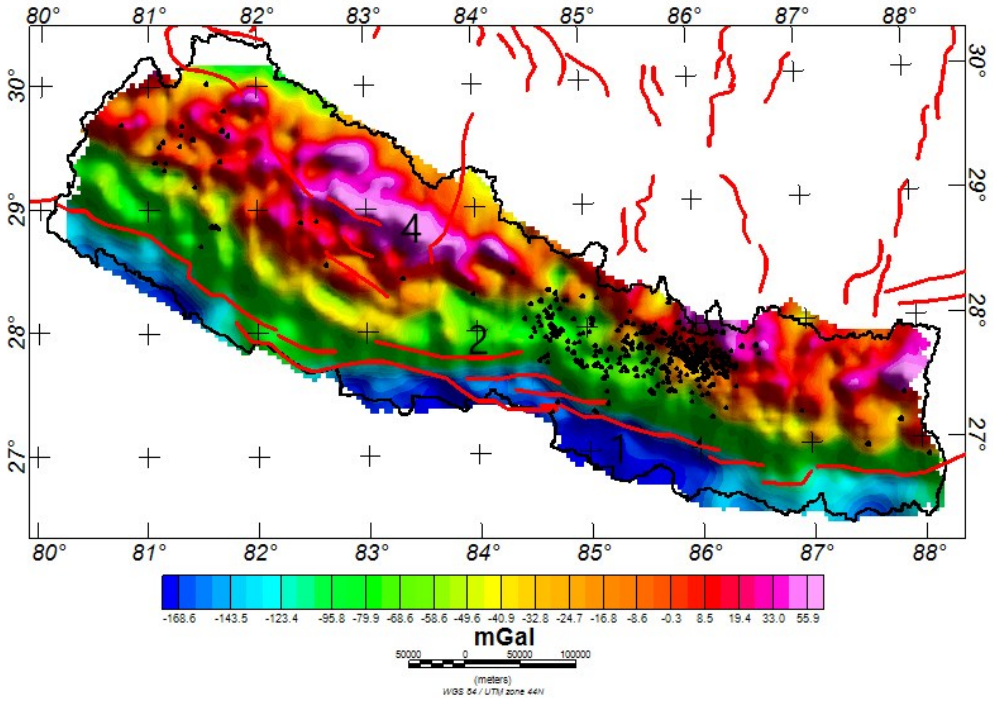

Figure 33 Isostatic residual gravity anomaly map of Nepal Himalaya. It is prepared by removing the isostatic regional gravity anomalies from the observed Bouguer gravity anomalies. A crustal thickness of 50km, the topographic density of 2.67g/cm^3, and Moho density of 3.3 g/cm^3 were used. The red lines represent the major fault boundaries. The black triangular shape represents the epicenter locations of the main shock and aftershocks of the 2015 Gorkha Earthquake area. Four distinct anomaly bodies are seen in the map which is grouped as 1(blue zone), 2(green zone), 3(red zone), and 4(pink zone).

To assist in determining the crustal structure, an isostatic residual anomaly map was created, which removed the gravity effects of the crustal thickening that became evident in the complete Bouguer gravity anomaly map. One can still see the steep gradient along the Main Boundary Thrust and the less dense (anomaly layer 2 in Figure 33) region where the Gorkha event occurred. This map (Figure 33) will be used in all further analyses.

5.2.2 Band-pass Filtered Gravity Anomaly Map: Wavelength filtering can be used to obtain the shorter wavelength residual gravity anomaly field (Peeples et al., 1986). This filtering method will isolate features of interest by removing the regional gravity effects in the upper

crust. Band-pass filtering is a type of wavelength filtering which allows only a certain range of wavelength between the upper cutoff limit and the lower cutoff limit (Lavin and Devane, 1970). Band pass filtering helps to bring out both longer and shorter wavelength anomalies using a single operation which consists of a combination of a high-pass filter and a low-pass filter.

A series of band-pass filtering maps of wavelength between 5 km and 150 km were prepared. Among these maps, one was picked which best fits the surface geology. Based on the correlation of geology and filtered gravity anomalies, the band-pass filtered map where wavelengths between 10 km and 120 km best matched with surface geology (Figure 34).

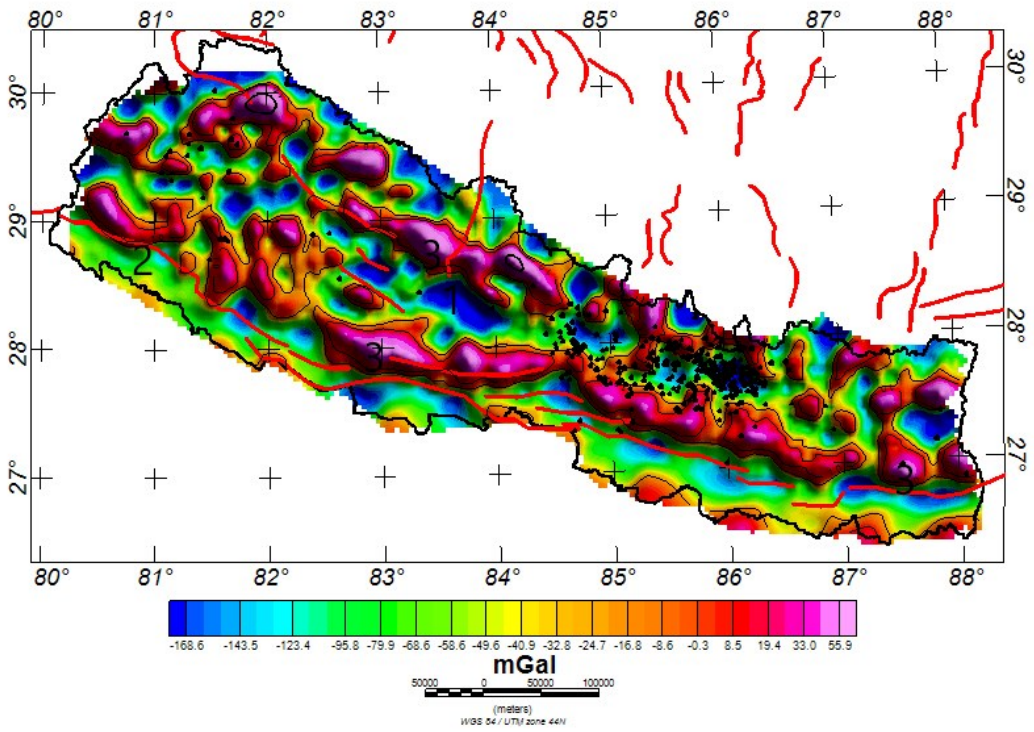

Figure 34 Band-pass filtered residual gravity anomaly map of the Nepal Himalaya determined by passing wavelength between 10 and 120 km. The red lines represent the major fault. The triangular black shape represents the epicenters of the main shock and aftershocks of the 2015 Gorkha earthquake. Three different anomaly layers can be seen in the map named 1(blue), 2(green), and 3(red to pink).

5.2.3 Derivative Gravity Anomaly Map: Derivative gravity anomaly maps are constructed to trace the outline of the edges of the subsurface density bodies (Blakely & Simpson, 1986; Blakely, 1995). There are different types of derivative methods including horizontal, vertical, and tilt derivatives. The horizontal derivatives are the calculation of the gradient anomaly in x- and y- direction over the edges of density contrast which helps to delineate the subsurface boundary zone (Grauch and Cordell, 1987; Fedi and Florio, 2002). The following formula was developed by Grauch and Cordell (1987) to design the THDR (Total Horizontal derivative) filter:

$$\text{THDR} = \sqrt{[(\partial T/\partial x)^2 + (\partial T/\partial y)^2]} \quad (1)$$

Where, T stands for the field, $\partial T/\partial x$ and $\partial T/\partial y$ stand for two horizontal derivatives of the field. Figure 35 represents the THDR of the area.

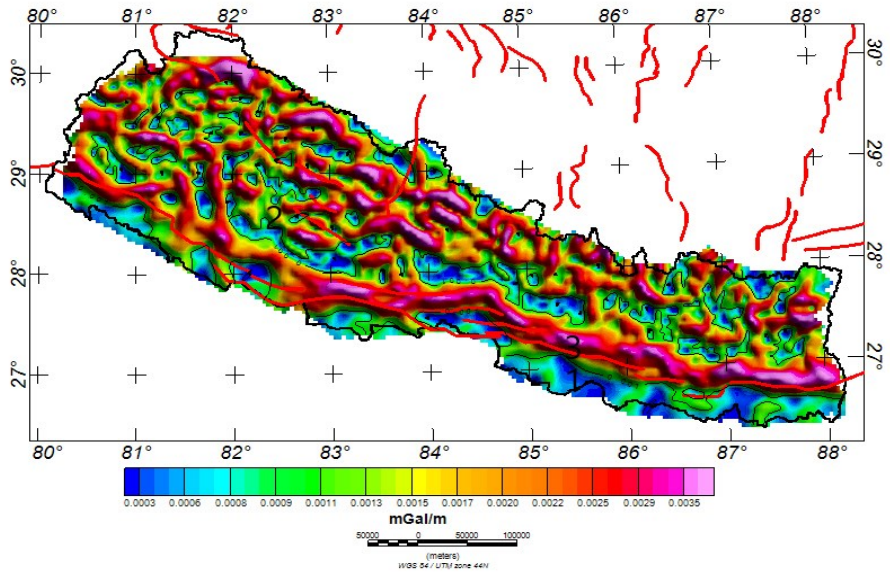

Figure 35 Total horizontal derivative gravity anomaly map of the Nepal Himalaya derived from isostatic residual gravity data. The red lines represent the major fault lines of the area. There are distinct three anomaly layers named 1(blue), 2(green), and 3(red to pink).

The horizontal derivative only gives the edges of the density body. The tilt derivative on the other hand is a linear equation to estimate the horizontal location and depth of source bodies using the source location parameter (Salem et al., 2008). The tilt derivative is based on the tilt angle (Miller and Singh, 1994; Verduzco et al., 2004) and is defined as the ratio of vertical derivative and the horizontal derivative (Dogru et al., 2017). The tilt angle is expressed as

$$TA = \tan^{-1}(\delta T/\delta Z/THDR) \quad (2)$$

Where, $\delta T/\delta Z$ represents the first order vertical derivative of the total gravity field.

This method is a grid-based method that can be used to determine a depth directly to a density source concerning the individual tilt of the gravity anomalies (Fairhead et al., 2011).

The tilt derivatives (Figure 36) were calculated on the Complete Bouguer gravity anomalies. The depths derived from the tilt derivative map show that most of the anomaly sources are at depths between 5-13 km.

5.2.4 Upward Continuation: The upward continuation method along with polynomial surface fitting can be used to approximate the regional gravity anomaly of an area (Kebede et al., 2020). Upward continuation transforms the potential fields from one elevation surface to a higher elevation surface which attenuates the shorter wavelength anomalies (Reynolds, 2011). Jacobsen (1987) developed an equation to show how to use upward continuation to remove the shallow anomaly sources. The gravity anomaly, Δgp, of the anomalous source at the upward continued surface point P (Figure 37) is,

$$\Delta gp = Gdmz/\ [(x-x0)2+(y-y0)2+\ (z+h)\ 2]3/2 \quad (3)$$

where, (x,y,z) are the coordinates of anomalous body, (x0,y0,z0) are the coordinates of the computed surface point, h is the height of the continued surface, G is an universal gravitational constant, and dm is the mass of the anomalous body.

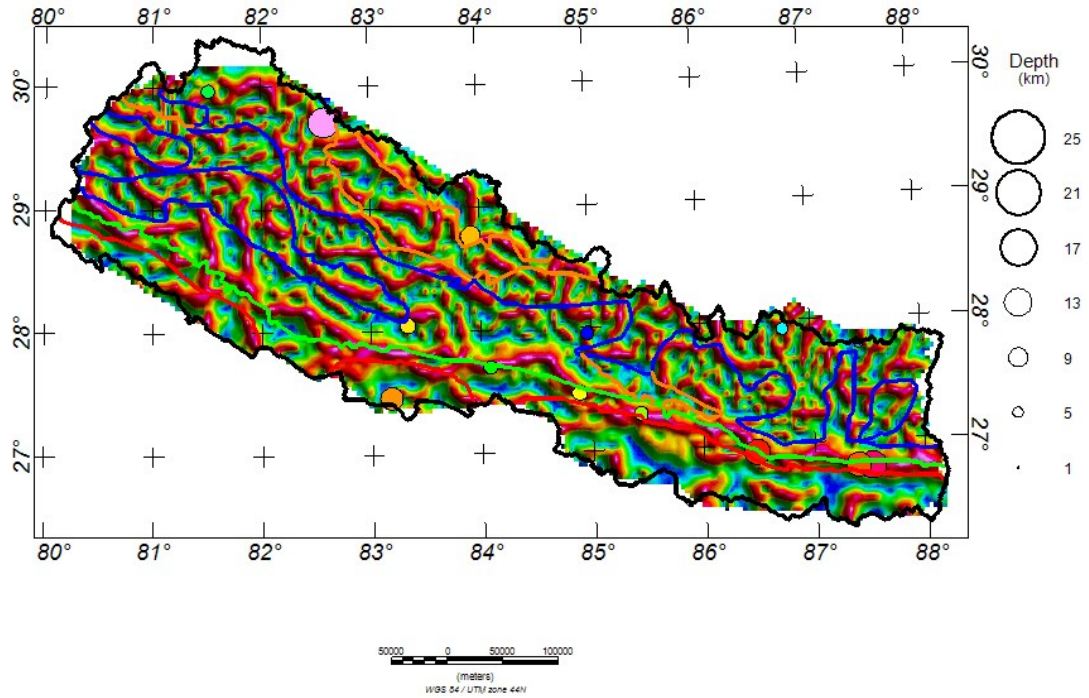

Figure 36 Tilt derivative gravity anomaly map of the Nepal Himalaya. The thick red line represents MFT, the green line represents MBT, blue represents MCT, and orange represents STDS. There are distinct three anomaly layers (blue, green, and red to pink). The depth of anomaly sources is represented by the circles. MFT= Main Frontal thrust, MBT= Main Boundary thrust, MCT= Main Central Thrust, and STDS= South Tibetan Detachment System.

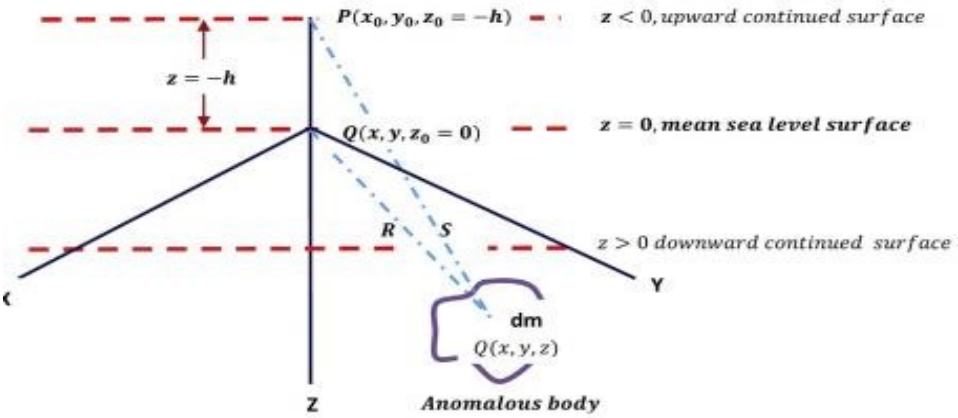

Figure 37 Diagrammatic representation of upward continuation technique in a cartesian coordinate system (Kebede et al., 2020).

To execute upward continuation, the complete Bouguer gravity anomaly data were continued upward to heights of 1 km, 5 km, 10 km, 20 km, 25 km, and 30 km respectively, using a constant removal of first-order polynomial surface (Figure 38). The pattern of disappearing shorter wavelength anomalies was continuously recorded to approximate the depth of the different anomaly sources. Jacobsen (1987) showed that the depth to an anomaly source is one-half or greater than the continuation distance.

5.2.5 Euler 3-D Deconvolution Method: Euler deconvolution is a popular method designed to locate the source and depths of magnetic and gravity anomalies (Reid et al., 1990; Reid et al., 2014). This method was first applied to magnetic data and later applied to gravity data (Thompson, 1982; Zhang et al., 2000). Euler's homogeneity equation is the main basis of the standard Euler's 3-D method (Thompson 1982) and is:

$$(x-xo)\,\delta T/\delta x + (y-yo)\,\delta T/\delta y + (z-zo)\,\delta T/\delta z = N\,(B-T) \quad (4)$$

Where, (xo, yo, zo) is the position of a source whose total field is detected at (x,y,z), B is the regional value of the field, and T is the total gravity field. The values $\delta T/\delta x$, $\delta T/\delta y$, and $\delta T/\delta z$ are the gravity gradient measurements along x-, y-, and z- directions whereas a non-negative integer N represents the SI (structural index) (Reid et al., 1990; Zhang et al., 2000).

The structural index (SI) is an important criterion in Euler deconvolution and is related to the local geology of a region (Reid et al., 1990). Reid et al. (2014) showed values of SI for different models and different data types. Using fractional SI value on the complex structure may produce misrepresentative results (Reid and Thurston, 2014). Reid et al. (2014) recommended choosing appropriate parameters to avoid errors in the results. For example, care must be given to select proper grid interval and a window size where the Euler equation is applied. They

proposed that the window size must be at least twice the original data spacing and more than half the desired depth of investigation. Table 3 shows recommend SI values (Reid et al., 2014).

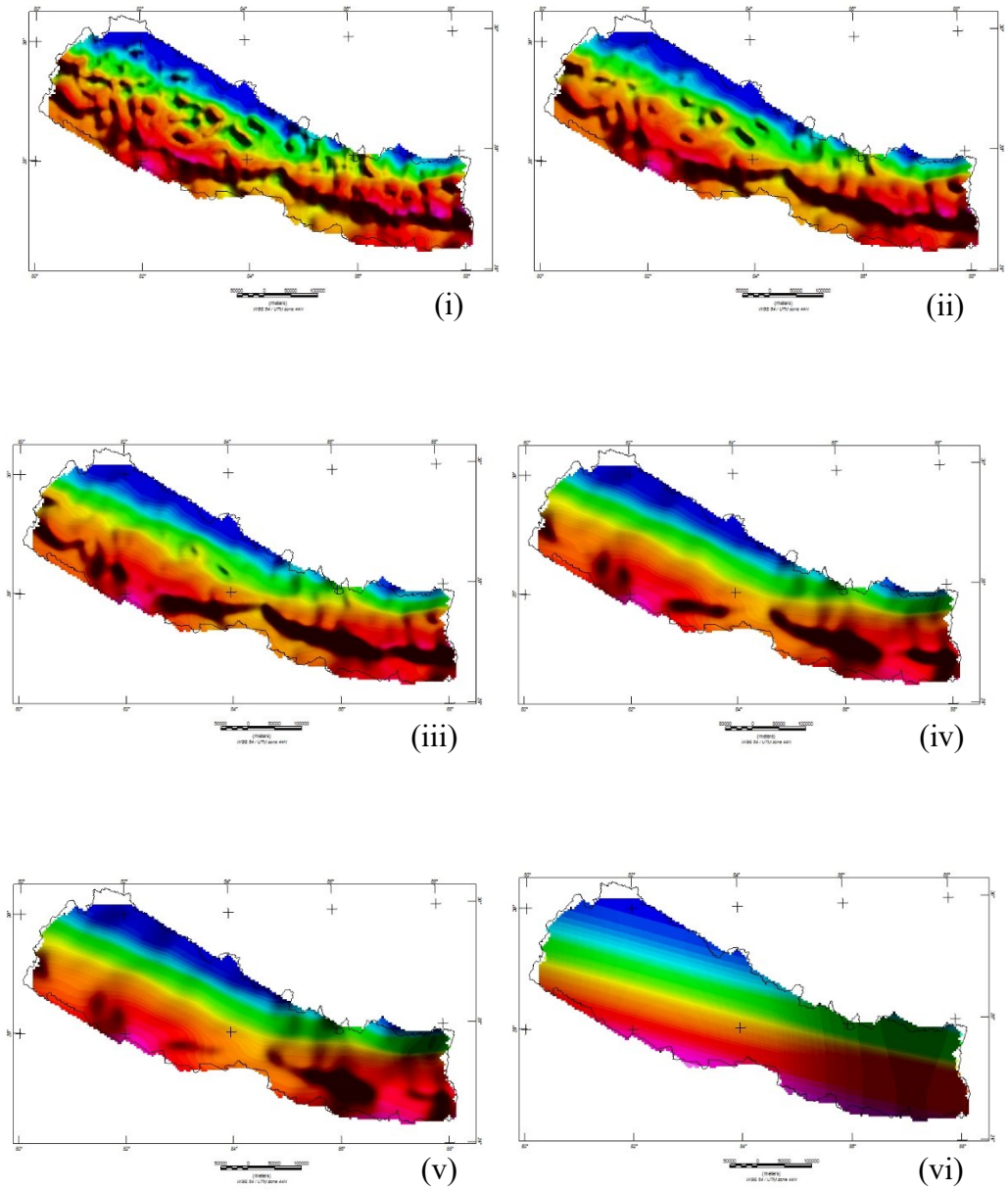

Figure 38 Bouguer gravity anomaly upward continuation map of the Nepal Himalaya. Bouguer gravity anomaly upward continued to (i) height of 1 km, (ii) height of 5 km, (iii) height of 10 km, (iv) height of 20 km, (v) height of 25 km, and (vi) height of 30 km, respectively.

For this study, a series of Euler's deconvolution maps were created by using a range of different SI values and window sizes. SI values of 0 and 1, window sizes of 10 km and 15 km were used. Similarly, the operations were used on the complete Bouguer gravity and the isostatic residual gravity anomaly maps. To administer the Euler deconvolution algorithm, the selected gravity data were first re-gridded at a 2 km spacing, after which the chosen parameter of SI and deconvolution window sizes were applied, and then horizontal and vertical gradient using the Fourier method were measured. Eight different Euler deconvolution depth solution maps were prepared from Bouguer gravity anomaly maps and isostatic residual anomaly maps with different SI (0 and 1) and window size (10 km and 15 km) values. An Euler depth solution map (Figure 39) constructed using the complete Bouguer gravity anomaly map with SI=1 and a window size of 15 km produced the best results as compared to the regional geology.

Table 3 Structural Index values for different structures from Reid et al. (2014).

Model	Magnetic SI	Gravity SI
Points, Sphere	3	2
Line, Cylinder, thin-bed fault	2	1
Thin sheet edge, thin sill, thin dyke	1	0
Thick sheet edge	0	-1[1]
Contact of infinite depth extent	0	Not useful[2]

[1] Requires the extended definition of SI and a non-linear deconvolution process.

[2] The gravity anomaly is infinite.

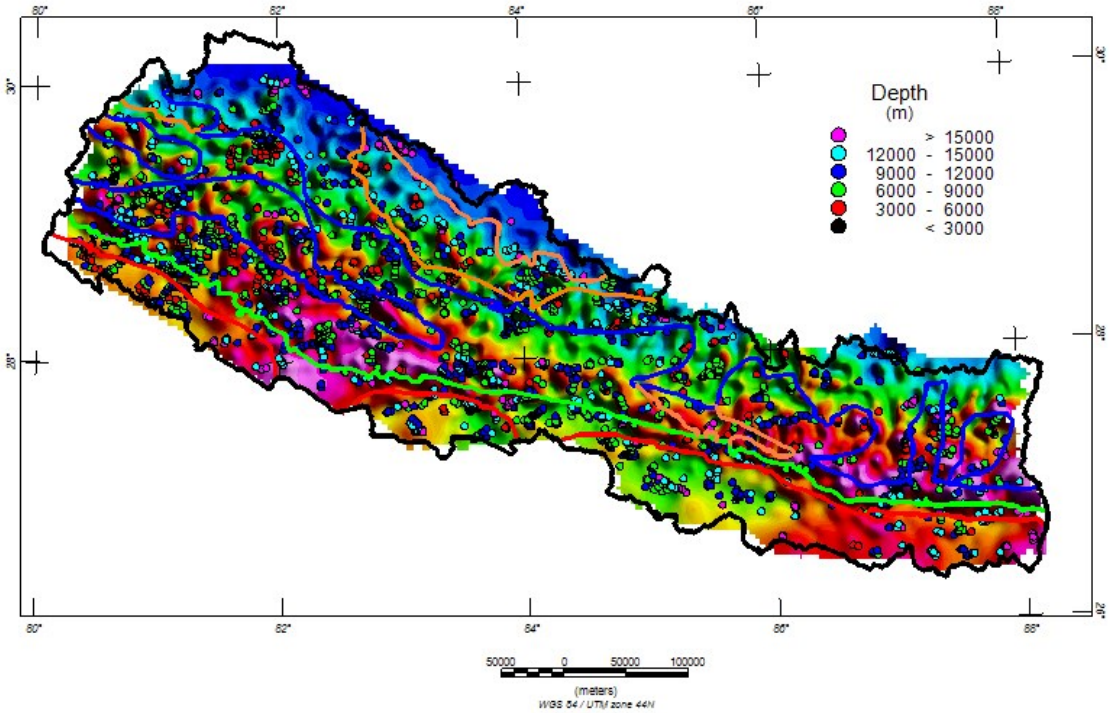

Figure 39 Euler deconvolution map of the Nepal Himalaya. Euler deconvolution solution map overlayed on the complete Bouguer gravity anomaly map. Euler solutions using a SI=1, and a window size of 15 km. The thick red line represents MFT, the green line represents MBT, blue represents MCT, and orange represents STDS. MFT-Main Frontal Thrust, MBT-Main Boundary Thrust, MCT- Main Central Thrust, and STDS-South Tibetan Detachment System.

CHAPTER-6 DISCUSSION

To interpret the gravity anomalies, a series of regional and residual gravity anomaly maps were constructed within and around the Central Nepal area. The gravity anomaly values observed in the Bouguer gravity anomaly map (Figure 30) were the reciprocal of the isostatic residual gravity anomaly map (Figure 33). This feature indicates that there are variable crustal density sources across the Nepal Himalayas. The complete Bouguer gravity anomaly values increase from north to south (Figure 30) which suggests they are related to crustal thickness decrease. The higher mountains in the north generate gravity minima and lower elevated lands in the southern part a gravity maximum. Therefore, the removal of the crustal cover from the complete Bouguer gravity data inverts the anomaly distribution across the area (Figure 33). The gravity minima represented by Anomaly 1(Figure 33) correlates with the Quaternary sediments of the Terai Zone (Figure 32). The low-density alluvium of the Indo-Gangetic Plain may produce this anomaly. The transitional zone between Anomaly 1 and Anomaly 2 (Figure 33) correlates with the Siwalik Zone. The loosely compacted sedimentary rocks followed by compacted sedimentary rocks might be the source of this anomaly. The thin sequence of the Siwalik Zone (Figure 32) could be the reason for the representation of the transition anomaly.

Gravity anomaly 2 (Figure 33) roughly correlates with the Lesser Himalaya Sequence except in Eastern Nepal. In Eastern Nepal, the Lesser Himalaya zone is thinner which may not produce a significant gravity anomaly. Low-grade metamorphic rocks in this region may be the origin of the anomaly.

The gravity maxima observed in the northern part of the isostatic residual gravity anomaly is correlated with the Higher Himalaya and Tethyan Himalayan geological sequences

(Figure 32). Anomaly 3 (Figure 33) correlates with most of the Higher Himalayan sequence. This thick sequence of high-grade metamorphic rocks is commonly dense and maybe the anomaly's source. There are several Paleozoic and Leucocratic granitic intrusions occurring in the Higher Himalayan sequence which could be represented as small patches of gravity minima intercalated with gravity maxima.

The gravity maxima (Anomaly 4) seen in the northern part of the Middle West region (Figure 33) correlates with the Tethyan Himalayan Sequences. Portions of the Tethyan sequences were related in Anomaly 3. This gravity maxima anomaly could be caused by the low to medium-grade marbles, quartzites, and limestones whereas the gravity maxima could be due to low-grade sedimentary sequences and Paleozoic granite intrusions. In Central Nepal, the Tethyan section is not noticeably correlated with the isostatic residual gravity anomaly map. Anomaly 2 occurs over the Tethyan sequences. The Crystalline Nappe and Klippe (Dhital, 2015) are found within this region and occur beneath the Tethyan sequence, which may be part of the anomaly's source. The isostatic residual gravity anomaly map (Figure 33) signifies that the source of this anomaly is likely to occur within the Lesser Himalayan sequences.

Wavelength filtering of the complete Bouguer gravity data was performed to highlight anomalies of different sources. Figure 34 is a band-pass filtered gravity anomaly map that indicates that most of the tectonic boundaries correlate with the gravity anomalies. This correlation between tectonic and gravity anomaly boundaries may reflect the different density contrast zones represented by respective tectonic divisions in the subsurface. The distribution of the gravity minima in between the gravity maxima is probably due to local geologic differences within the large-scale tectonic boundaries (Figure 5). One can also notice that most of the epicenter of the mainshock and aftershocks of the 2015 Gorkha earthquake lies within the gravity

anomaly contrast region (Figure 33). This gravity anomaly contrast and increasing gravity gradient within the earthquake region suggest that various crustal structures within the region control the earthquake rupture direction and focus location. The analysis indicates the crust in the region of the 2015 Gorkha Earthquake is less dense than the region to the west and east suggesting the large-scale density differences played a role in stress isolation within the region.

The edge of the density body can be determined by using horizontal or vertical derivates (Blakely and Simpson, 1986). The THDR map (Figure 35) exhibits the same derivative maxima and minima pattern as the bandpass filter map (Figure 34) but the edges of the anomaly sources are narrower. The anomaly zone that correlates with the Siwalik zone is seen thinner than in the bandpass filter map which could explain that the edges of the source body representing Siwalik zones are thinner than the surface representation. The gravity gradient at the Siwalik zone in the Central Nepal region is calculated as 2.7 mGal/km from the Indo-Gangetic plain, whereas the gravity gradient at the Lesser Himalaya zone is 0.9 mGal/km from the Siwalik zone. Similarly, the gravity gradient at the Higher Himalaya from Lesser Himalaya in central Nepal is 2.2 mGal/km. The steeper gradient can be defined as the deeper and steeper Moho (Lyon-Caen and Molnar, 1985). So, the Moho is deeper beneath the Siwalik zone than beneath the Indo-Gangetic Plain and it is deeper beneath the Higher Himalaya zone than in the Lesser Himalaya zone. The edge and depth of the source body, estimated from a tilt derivative map (Salem et al., 2008), (Figure 36) shows the same edges of the density source bodies as shown on the THDR map (Figure 35). The THDR map also can provide depth to density sources. The analysis indicates a wide range of depths between 5-17 km occurs along with the MFT. The depth to the sources within the MHT is between 5 to 17 km as the front portion of these depths correlates with the

MHT. This agrees with Hossain et al. (2015) who found similar depths of the MHT before the locking zone (Figure 12).

The depth source of anomalies can also be detected using the upward continuation technique (Jacobson, 1987) where a gravity field can be calculated at different elevation surfaces. Upward continuation to higher elevations will attenuate shorter wavelength anomalies. Additionally, Jacobsen (1987) showed that the depth to the source of an anomaly is one-half of the continuation distance when that anomaly is removed. The upward continuation of the complete Bouguer gravity anomalies to 1 km (Figure 38, (i)) indicates that almost all the anomalies are still the same as those on the complete Bouguer gravity anomaly map (Figure 30). But when the continuation elevation was increased different anomaly features gradually disappeared. Careful tracking of continuation height and disappearing anomalies helped identify the depth of the anomaly source. Most of the small-scale anomaly features were removed when the data were upward continued to 10 km and almost all anomaly features were removed when continued to 30 km (Figure 38). This implies that most anomaly sources lie between the depths of 5 to 10 km.

The depth information implied using the upward continuation maps is closely tied up with the depth solutions determined by 3D Euler's deconvolution analysis. The Euler's deconvolution of the complete Bouguer gravity anomalies using a structural index of 1 and a window size of 15 km indicated a systematic clustering of depth values ranging from 3 km to 12 km. This clustering implies that the anomalies observed on the isostatic residual gravity anomaly map are caused by density sources laying between 3 km to 12 km in depth. The solution depths greater than 15 km are not systematically clustered. In general, a solution depth twice the window size can be considered the depth of the anomaly source (Reid et al., 2014). So, any depth

solution less than 30 km can be considered here as a possible depth of the density source. However, a depth solution greater than 15 km would be a rare occurrence. Euler's depth solutions in correlation with the gravity gradients (Figure 39) also give some clues about the distribution of the density bodies. The depth solutions along the MFT line indicate that the depths range from 3 km to more than 15 km. The THDR map also interprets the MHT depth to range between 5- 17 km. The seismic wave from modeling and multiscale double-difference earthquake relocations study of Bai et al. (2016) also revealed similar depth ranges of MHT. So, the depth range of MHT can be interpreted as 3-17 km before the locking zone.

CHAPTER-7 CONCLUSION

The Nepal Himalaya is one of the most significant tectonic zones within the Himalaya Orogeny. It is subdivided into five major geotectonic divisions: Terai zone, Siwalik zone, Lesser Himalaya zone, Higher Himalaya zone, and Tethys Himalayan zone. These geotectonic divisions are separated from each other by four major mega-fault systems: MFT, MBT, MCT, and STDS. An analysis of the available land and airborne gravity data within Nepal, including the 2015 Gorkha Earthquake regions of the Central Nepal area, was used to determine the relationship between the tectonic divisions and density sources within the crust. Complete Bouguer Gravity, isostatic residual, band-pass filter, total horizontal derivative, tilt derivative, upward continued and Euler's deconvolution maps were constructed to analyze the gravity data associated with the Nepal Himalaya tectonic zonation. The Nepal Himalaya is characterized by a south to north-trending gravity gradient due to the crustal thickening from south to north. The removal of the crustal thickening by the isostatic residual anomaly technique produced a series of gravity maxima and minima associated with these major tectonic divisions.

The combination of low- and high-pass filtered maps and the isostatic residual gravity anomaly map showed that the pattern of major tectonic boundaries and the gravity anomalies boundaries are correlated, suggesting that these tectonic zones have different density values. The correlation between the major fault boundaries and the isostatic residual gravity anomalies also strengthened the relationship between the density sources associated with the tectonic zones. Most of the epicenter locations of the mainshock and aftershocks of the 2015 Gorkha Earthquake were centered within the high gravity gradient region also indicating that large-scale density differences played a role in stress isolation within the region.

Derivative maps determined that the edge of subsurface density sources is thinner than the surface representation in the Complete Bouguer and isostatic residual gravity anomaly maps. This indicates that the density sources become thinner at depth. The tilt derivative map, upward continued map and Euler's deconvolution map agree that most of the density sources are between 3 km and 15 km in depth. The depth solutions along the MFT revealed that the depth of MHT ranges from 3 km to 17 km before the locking zone between the Indian plate and Eurasian plate. The steeper gradient of the anomaly from north to the south indicates the Moho is steeper and deeper towards the north.

This study gives the source location and distribution of the different gravity anomalies. The geometry and the exact location of different subsurface density structures like lithospheric structure and Moho can be edge out from 2-D gravity modeling of the cross-section profiles of Euler's deconvolution map concerning seismic and geology constraints. This 2-D gravity model of Central Nepal will give further insight into the crustal structure of the 2015 Gorkha Earthquake region.

REFERENCES

Acharya, K.K., 2008, Qualitative Kinematic Investigations related to the Extrusion of the Higher Himalayan Crystalline and Equivalent Tectonometamorphic Wedges in the Central Nepal Himalaya: PhD dissertation in Geology, University Wien, Austria, 165 p.

Ahmad, T., Harris, N., Bickle, M., Chapman, H., Bunbury, J., and Prince, C., 2000, Isotopic constraints on the structural relationships between the Lesser Himalayan Series and the High Himalayan Crystalline Series, Garhwal Himalaya: Bulletin of the Geological Society of America, v. 112, p. 467–477, doi:10.1130/0016-7606(2000)112<467:ICOTSR>2.0.CO;2.

Auden, J.B., 1935, Traverses in the Himalaya: Records of Geological survey of India, v. 69, p. 123-167.

Bai, L., Klemperer, S.L., Mori, J., Karplus, M.S., Ding, L., Liu, H., Li, G., Song, B., and Dhakal, S., 2019, Lateral variation of the Main Himalayan Thrust controls the rupture length of the 2015 Gorkha earthquake in Nepal: Science Advances, v. 5, p. 1–8, doi:10.1126/sciadv.aav0723.

Bai, L., Liu, H., Ritsema, J., Mori, J., Zhang, T., Ishikawa, Y., and Li, G., 2016, Faulting structure above the Main Himalayan Thrust as shown by relocated aftershocks of the 2015 Mw7.8 Gorkha, Nepal, earthquake: Geophysical Research Letters, v. 43, p. 637–642, doi:10.1002/2015GL066473.

Bashyal, R.P., 1998, Petroleum exploration in Nepal: Journal of Nepal Geological Society, v. 18, p. 19-24.

Bilham, R., 2015. Raising Kathmandu: Nature Geoscience, v. 8, p. 582-584.

Bilham, R., Gaur, V.K. and Molnar, P., 2001, Himalayan seismic hazard: Science, v. 293, p. 1442-1444.

Bilham, R. et al., 1997, GPS measurements of present-day convergence across the Nepal Himalaya: Nature, v. 386, p. 61–64, doi:10.1038/386061a0.

Blakely, R. J., 1995, Potential Theory in Gravity & Magnetic Applications: Cambridge University Press, New York.

Blakely, R.J., and Simpson, R.W., 1986, Approximating edges of source bodies from magnetic or gravity anomalies.: Geophysics, v. 51, p. 1494–1498, doi:10.1190/1.1442197.

Cattin, R., Martelet, G., Henry, P., Avouac, J.P., Diament, M., and Shakya, T.R., 2001, Gravity anomalies, crustal structure and thermo-mechanical support of the Himalaya of Central Nepal: Geophysical Journal International, v. 147, p. 381–392, doi:10.1046/j.0956-540X.2001.01541.x.

CHAUDHRY, R., 1982, Petrology of the Siwalik group of Nepal Himalaya: Recent researches in geology.

Chen, S., Liu, M., Xing, L., Xu, W., Wang, W., Zhu, Y., and Li, H., 2016, Gravity increase before the 2015 Mw 7.8 Nepal earthquake: Geophysical Research Letters, v. 43, p. 111–117, doi:10.1002/2015GL066595.

Colchen, M., Le Fort, P. and Pêcher, A., 1986, Recherches géologiques dans l'Himalaya du Népal. Annapurna, Manaslu, Ganesh: Edition du CNRS, Paris (éd. bilingue), 136p.

Dal Zilio, L., Jolivet, R., and van Dinther, Y., 2020, Segmentation of the Main Himalayan Thrust Illuminated by Bayesian Inference of Interseismic Coupling: Geophysical Research Letters, v. 47, p. 1–10, doi:10.1029/2019GL086424.

DeCelles, P.G., Gehrels, G.E., Quade, J., LaReau, B., and Spurlin, M., 2000, Tectonic implications of U-Pb zircon ages of the Himalayan orogenic belt in Nepal: Science, v. 288, p. 497–499, doi:10.1126/science.288.5465.497.

DeCelles, P.G., Gehrels, G.E., Quade, J., and Ojha, T.P., 1998, Eocene-early Miocene foreland basin development and the history of Himalayan thrusting, western and central Nepal: Tectonics, v. 17, p. 741–765, doi:10.1029/98TC02598.

Denolle, M.A., Fan, W., and Shearer, P.M., 2015, Dynamics of the 2015 M7.8 Nepal earthquake: Geophysical Research Letters, v. 42, p. 7467–7475, doi:10.1002/2015GL065336.

Dhakal, S., Bai, L., Neupane, B., Li, L., and Song, B., 2019, Review of earthquake activity and faulting structure in Nepal Himalaya: Bulletin of Nepal Geological Society, v. 36, p. 259–266.

Dhakal, S., 2016, Disasters in Nepal: Disaster Risk Management, p. 39–74.

Dhital, M.R., 2015, Geology of the Nepal Himalaya: regional perspective of the classic collided orogen: Springer.

DOGRU, F., PAMUKCU, O. and OZSOZ, I., 2017, Application of tilt angle method to the Bouguer gravity data of Western Anatolia: Maden Tetkik ve Arama Dergisi, v. 155, p. 213-222.

Duba, K., 2018, Crustal Structure of the Bhutanese Himalaya: New Insights from a Gravity Analysis in Western and Central Bhutan: Crustal Structure of the Bhutanese Himalaya: New Insights from a Gravity Analysis in Western and Central Bhutan, p. 3240, https://bearworks.missouristate.edu/theseshttps://bearworks.missouristate.edu/theses/3240.

Fairhead, J.D., Salem, A., Cascone, L., Hammill, M., Masterton, S., and Samson, E., 2011, New developments of the magnetic tilt-depth method to improve structural mapping of

sedimentary basins: Geophysical Prospecting, v. 59, p. 1072–1086, doi:10.1111/j.1365-2478.2011.01001.x.

Fedi, M. and Florio, G., 2002, A stable downward continuation by using the ISVD method: Geophysical Journal International, v. 151, p.146-156.

Forsberg, R., Olesen, A.V., Einarsson, I., Manandhar, N. and Shreshta, K., 2014, Geoid of Nepal from airborne gravity survey: Earth on the Edge: Science for a Sustainable Planet, Springer, Berlin, Heidelberg, p. 521-527.

Gansser, A., 1964, Geology of the Himalaya: Wiley- Interscience, New York, 289 p.

Gansser, A., 1983, Geology of the Bhutan Himalaya: Birkhauser Verlag, Boston, 181 p.

Godin, L., Grujic, D., Law, R.D., and Searle, M.P., 2006, Channel flow, ductile extrusion and exhumation in continental collision zones: An introduction: Geological Society Special Publication, v. 268, p. 1–23, doi:10.1144/GSL.SP.2006.268.01.01.

Grandin, R., Vallée, M., Satriano, C., Lacassin, R., Klinger, Y., Simoes, M., and Bollinger, L., 2015, Rupture process of the Mw = 7.9 2015 Gorkha earthquake (Nepal): Insights into Himalayan megathrust segmentation: Geophysical Research Letters, v. 42, p. 8373–8382, doi:10.1002/2015GL066044.

Grauch, V.J.S. and Cordell, L., 1987, Limitations of determining density or magnetic boundaries from the horizontal gradient of gravity or pseudogravity data: Geophysics, v. 52, p. 118-121.

Gurung, D., 1998, Freshwater molluscs from the Late Neogene Siwalik Group, Surai Khola, western Nepal: Journal of the Nepal Geological Society, v. 17, p.7-28.

Hagen, T. and Hunger, J.P., 1952, Über geologisch-petrographische Untersuchungen in zentral-Nepal: Leemann.

Hagen, T., 1969, Report on the geological survey of Nepal, vol. 1.

Hauck, M.L., Nelson, K.D., Brown, L.D., Zhao, W., and Ross, A.R., 1998, Crustal structure of the Himalayan orogen at -90° east longitude from Project INDEPTH deep reflection profiles: Tectonics, v. 17, p. 481–500, doi:10.1029/98TC01314.

He, R., Liu, G., Golos, E., Gao, R., and Zheng, H., 2014, Isostatic gravity anomaly, lithospheric scale density structure of the northern Tibetan plateau and geodynamic causes for potassic lava eruption in Neogene: Tectonophysics, v. 628, p. 218–227, doi:10.1016/j.tecto.2014.04.047.

Hetényi, G. et al., 2016, Segmentation of the Himalayas as revealed by arc-parallel gravity anomalies: Scientific Reports, v. 6, p. 1–10, doi:10.1038/srep33866.

Hossain, A.S.M., Adhikari, T.L., Ansary, M.A., and Bari, Q.H., 2015, Characteristics and consequence of Nepal earthquake 2015: A review: Geotechnical Engineering, v. 46, p. 114–120.

Huang, Y., Yang, S., Qiao, X., Lin, M., Zhao, B. and Tan, K., 2017, Measuring ground deformations caused by 2015 Mw7. 8 Nepal earthquake using high-rate GPS data: Geodesy and Geodynamics, v. 8, p. 285-291.

Hubbard, J., Almeida, R., Foster, A., Sapkota, S.N., Bürgi, P., and Tapponnier, P., 2016, Structural segmentation controlled the 2015 MW 7.8 Gorkha earthquake rupture in Nepal: Geology, v. 44, p. 639–642, doi:10.1130/G38077.1.

Jacobsen, B.H., 1987, Case for Upward Continuation As a Standard Separation Filter for Potential-Field Maps.: Geophysics, v. 52, p. 1138–1148, doi:10.1190/1.1442378.

Kargel, J.S. et al., 2016, Geomorphic and geologic controls of geohazards induced by Nepal's 2015 Gorkha earthquake: Science, v. 351, doi:10.1126/science.aac8353.

Kebede, H., Alemu, A., and Fisseha, S., 2020, Upward continuation and polynomial trend analysis as a gravity data decomposition, case study at Ziway-Shala basin, central Main Ethiopian rift: Heliyon, v. 6, p. e03292, doi:10.1016/j.heliyon.2020.e03292.

Kono, M., 1974, Gravity Anomalies in East Nepal and their Implications to the Crustal Structure of the Himalayas: Geophysical Journal of the Royal Astronomical Society, v. 39, p. 283–299, doi:10.1111/j.1365-246X.1974.tb05455.x.

Lavin, P.M. and Devane, J.F., 1970. Direct design of two-dimensional digital wavenumber filters: Geophysics, v. 35, p. 1073-1078.

Le Fort, P., 1975, Himalayas: the collided range. Present knowledge of the continental arc: American Journal of Science, v. 275, p. 1–44.

Le Fort, P., 1975 a, The anatectic Himalayan leucogranites with emphasis on the Manaslu tourmaline granite: Recent researches in geology, v. 2, p. 76-90.

Le Fort, P., 1986, The 500 Ma magmatic event in Alpine southern Asia, a thermal episode at Gondwana scale: Evolution des Domaines Orogeniques d'Asie Meridionale, v. 47, p. 191-209.

Lingshun, M., Ye, G., Li, Q. and Rui, G., 1995, Gravity field and deep crustal structure in Golmud-Ejin Qi Geoscience Transection and nearby area [J]: Chinese J. Geophys, v. 38(Supp. II), p. 36-45.

Lyon-Caen, H., and Molnar, P., 1985, Gravity anomalies, flexure of the Indian Plate, and the structure, support and evolution of the Himalayan and Ganga Basin: Tectonics, v. 4, p. 513-538, doi: 10.1029/ TC004i006p00513.

Manandhar, N., and Shanker, K.C. Geoid Determination and Gravity Works in: v. 14, p. 7–15.

Martin, A. J., 2017, A review of Himalayan stratigraphy, magmatism, and structure: Gondwana Research, v. 49, p. 42-80.

McQuarrie, N., Robinson, D., Long, S., Tobgay, T., Grujic, D., Gehrels, G., and Ducea, M., 2008, Preliminary stratigraphic and structural architecture of Bhutan: Implications for the along strike architecture of the Himalayan system: Earth and Planetary Science Letters, v. 272, p. 105–117, doi:10.1016/j.epsl.2008.04.030.

Medlicott, H.B., Blanford, W.T., Ball, V. and Mallett, F.R., 1879, A Manual of the Geology of India: Peninsular area.

Mickus, K., and Jallouli, C., 1999, Crustal structure beneath the Tell and Atlas Mountains (Algeria and Tunisia) through the analysis of gravity data: Tectonophysics, v. 314, p. 373–385, doi:10.1016/S0040-1951(99)00225-5.

Miller, H.G. and Singh, V., 1994, Potential field tilt—a new concept for location of potential field sources: Journal of applied geophysics, v. 32, p. 213-217.

Murthy, I.R. and Rao, S.J., 1994, Gravity inversion of horizontal circular discs and vertical circular cylinders: Computers & Geosciences, v. 20, p. 821-838.

Nábělek, J., Hetényi, G., Vergne, J., Sapkota, S., Kafle, B., Jiang, M., Su, H., Chen, J., Huang, B. S., and the Hi-CLIMB Team, 2009, Underplating in the Himalaya-Tibet Collision zone revealed by Hi-CLIMB experiment: Science, v. 325, p. 1371-1374.

Ni, J. and Barazangi, M., 1984, Seismotectonics of the Himalayan collision zone: Geometry of the underthrusting Indian plate beneath the Himalaya: Journal of Geophysical Research: Solid Earth, v. 89, p. 1147-1163.

Ni, J.F., 1989, Active tectonics of the Himalaya: Proceedings of the Indian Academy of Sciences-Earth and Planetary Sciences, v. 98, p. 71-89.

Oli, L.M., Paudel, S., and Paudel, L.P., 2019, Metamorphism of Jhyallaphay-Barpak-Bhachchek area of Gorkha District, Lesser Himalaya and Higher Himalaya, Central Nepal: Journal of Nepal Geological Society, v. 58, p. 119–130, doi:10.3126/jngs.v58i0.24595.

Patriat, P. and Achache, J., 1984, India–Eurasia collision chronology has implications for crustal shortening and driving mechanism of plates: Nature, v. 311, p. 615-621.

Peeples, W.J., Coultrip, R.L. and Keller, G.R., 1986, Quasi-ideal spatial filters for large maps: Annales geophysicae. Series B. Terrestrial and planetary physics, v. 4, no. 5, p. 547-553.

Prakash, R., Singh, R.K. and Srivastava, H.N., 2016, Nepal earthquake 25 April 2015: source parameters, precursory pattern and hazard assessment: Geomatics, Natural Hazards and Risk, v. 7, p. 1769-1784.

Quade, J., Cater, J.M.L., Ojha, T.P., Adam, J., and Harrison, T.M., 1995, Late Miocene environmental change in Nepal and the northern Indian subcontinent: stable isotopic evidence from paleosols: Geological Society of America Bulletin, v. 107, p. 1381–1397, doi:10.1130/0016-7606(1995)107<1381:LMECIN>2.3.CO;2.

Rai, S.M., 2001, Geology, geochemistry and radiochronology of the Kathmandu and Gosainkund Crystalline nappes, central Nepal Himalaya: Journal of Nepal Geological Society, v. 25, p. 135–155.

Rai, S.M., Guillot, S., Le Fort, P. and Upreti, B.N., 1998, Pressure–temperature evolution in the Kathmandu and Gosainkund regions, Central Nepal: Journal of Asian Earth Sciences, v. 16, p. 283-298.

Reid, A.B., Ebbing, J., and Webb, S.J., 2014, Avoidable Euler Errors - the use and abuse of Euler deconvolution applied to potential fields: Geophysical Prospecting, v. 62, p. 1162–1168, doi:10.1111/1365-2478.12119.

Reid, A.B., Allsop, J.M., Granser, H., Millett, A.T. and Somerton, I.W., 1990, Magnetic interpretation in three dimensions using Euler deconvolution: Geophysics, v. 55, p. 80-91.

Reid, A.B., Ebbing, J. and Webb, S.J., 2014, Avoidable Euler errors–the use and abuse of Euler deconvolution applied to potential fields: Geophysical Prospecting, v. 62, p. 1162-1168.

Reynolds, J.M., 2011, An introduction to applied and environmental geophysics: John Wiley & Sons.

Roy, A.B. and Purohit, R., 2018, Chapter 2—Indian Subcontinent: Geomorphic and Geophysical Traits: Elsevier: Amsterdam, The Netherlands, p. 13-30.

Sakai, H., Fujii, R., Sugimoto, M., Setoguchi, R., and Paudel, M.R., 2016, Two times lowering of lake water at around 48 and 38 ka, caused by possible earthquakes, recorded in the Paleo-Kathmandu lake, central Nepal Himalaya: Earth, Planets and Space, v. 68, doi:10.1186/s40623-016-0413-5.

Salem, A., Williams, S., Fairhead, D., Smith, R., and Ravat, D., 2008, Interpretation of magnetic data using tilt-angle derivatives: Geophysics, v. 73, doi:10.1190/1.2799992.

Sastry, R.G., and Singh, V.P. Crustal Structure of NW Himalaya through Gravity and Magnetic Data Analysis: , p. 2–6.

Scott, W., Leaney, P. and Ulrych, T.J., 1987, Multiple dynamic matching: a new approach to well log correlation: Geoexploration, v. 24, p. 503-515.

Searle, M.P. and Searle, M., 2013, Colliding continents: a geological exploration of the Himalaya, Karakoram, and Tibet: Oxford University Press.

Searle, M.P., and Treloar, P.J., 2019, Introduction to Himalayan tectonics: A modern synthesis: Geological Society Special Publication, v. 483, p. 1–17, doi:10.1144/SP483-2019-20.

Simpson, R.W., Jachens, R.C., Blakely, R.J. and Saltus, R.W., 1986, A new isostatic residual gravity map of the conterminous United States with a discussion on the significance of isostatic residual anomalies: Journal of Geophysical Research: Solid Earth, v. 91, p. 8348-8372.

Singh, B.P., Bhargava, O.N., Mikuláš, R., Prasad, S.K., Morrison, S., Chaubey, R.S., and Kishore, N., 2019, Discovery of traces of Cruzianasemiplicata and C. Rugosa groups (cambro-ordovician) from the lesser Himalaya, India and their stratigraphic, tectonic and palaeobiogeographic implications: Journal of the Palaeontological Society of India, v. 64, p. 283–303.

Srivastava, P. and Mitra, G., 1994, Thrust geometries and deep structure of the outer and lesser Himalaya, Kumaon and Garhwal (India): Implications for evolution of the Himalayan fold-and-thrust belt: Tectonics, v. 13, p. 89-109.

Stöcklin, J. and Bhattarai, K.D., 1977, Geology of the Kathmandu area and central Mahabharat range, Nepal Himalaya: Report of Department of Mines and Geology/UNDP(unpublished), 86p.

Stöcklin, J., 1980, Geology of Nepal and its regional frame: Thirty-third William Smith Lecture: Journal of the Geological Society, v. 137, p. 1-34.

Subedi, L. and Acharya, K.K., 2016, Tracing the Mahabharat Thrust (MT) on the basis of lithology and microstructures around Bhainse-Manahari area, central Nepal: Journal of Nepal Geological Society, v. 51, p. 39-48.

Takada, Y, and Matsu'ura, M., 2007, Geometric evolution of plate interface-branch fault system: Its effects on the tectonic development of the Himalayas: Journal of Asian Earth Sciences, v. 29, p. 490-503.

Takayasu, K., 1988, Freshwater molluscan fossils from the Churia (Siwalik) Group and the rising Himalayas: Himalayan Upheaval, p. 81-93.

Thakur, V.C., Joshi, M., and Jayangondaperumal, R., 2020, Active tectonics of Himalayan frontal fault zone in the sub-Himalaya: Springer Geology, p. 439–466, doi:10.1007/978-3-030-15989-4_12.

Thapa, D.R., 2018, Seismicity of Nepal and the Surrounding Region: Bulletin of the Department of Geology, v. 20, p. 83–86, doi:10.3126/bdg.v20i0.20727.

Thapa, D.R., Tao, X., Wang, G., and Fan, F., 2017, Deterministic seismic hazard assessment for Nepal: Sixteenth World Conference on Earthquake Engineering, p. 1–8.

Thompson, D.T., 1982, EULDPH: a new technique for making computer-assisted depth estimates from magnetic data.: Geophysics, v. 47, p. 31–37, doi:10.1190/1.1441278.

Upreti, B.N. and Le Fort, P., 1999, Lesser Himalayan crystalline nappes of Nepal: Problems of their origin: SPECIAL PAPERS-GEOLOGICAL SOCIETY OF AMERICA, p. 225-238.

Upreti, B. N., 1999, An overview of the stratigraphy and tectonics of the Nepal Himalaya: Journal of Asian Earth Science, v. 17, p. 577-606.

Valdiya, K.S., 1980, The two intracrustal boundary thrusts of the Himalaya: Tectonophysics, v. 66, p. 323-348.

Verduzco, B., Fairhead, J.D., Green, C.M. and MacKenzie, C., 2004, New insights into magnetic derivatives for structural mapping: The leading edge, v. 23, p. 116-119.

Wang, K., and Fialko, Y., 2015, Slip model of the 2015 Mw 7.8 Gorkha (Nepal) earthquake from inversions of ALOS-2 and GPS data: Geophysical Research Letters, v. 42, p. 7452–7458, doi:10.1002/2015GL065201.

Wu, Z., Barosh, P.J., Ha, G., Yao, X., Xu, Y. and Liu, J., 2019, Damage induced by the 25 April 2015 Nepal earthquake in the Tibetan border region of China and increased post-seismic hazards: Natural Hazards and Earth System Sciences, v. 19, p. 873-888.

Zhang, C., Mushayandebvu, M. F., Reid, A. B., Fairhead, J. D. and Odegard, M. E., 2000, Euler deconvolution of tensor gradient gravity data: Geophysics, v. 65, p. 512–520.

Zhang, Y.Q., Wang, Q.S. and Teng, J.W., 2010, The crustal isostatic anomaly beneath eastern Tibet and western Sichuan and its relationship with the distribution of earthquakes: Diqiu Wuli Xuebao, v. 53, p. 2631-2638.

Zhao, W., Nelson, K.D., Che, J., Quo, J., Lu, D., Wu, C. and Liu, X., 1993, Deep seismic reflection evidence for continental underthrusting beneath southern Tibet: Nature, v. 366, p. 557-559.